Thermochimica Acta, 238 (1994) 113–154
Elsevier Science B.V., Amsterdam
SSDI 0040-6031(93)01578-Q

A description of melting and crystallization of eutectic oligomers and copolymers — an application of the physical concepts of colloids

H.G. Kilian
Abteilung Experimentelle Physik, Universität Ulm (Germany)

(Received 4 March 1993; accepted 25 October 1993)

Abstract

A thermodynamic treatment of eutectoid crystallization in oligomer mulit-component systems comprised of homologues allows isobaric state diagrams to be predicted. This description relies on the definition of an inhomogeneous extended-chain micro-phase. The thickness distribution of crystals and the chain-length distribution are strictly interrelated because chain ends are squeezed into defect layers. The clear possibilities of a quantitative thermal analysis of melting in eutectoid oligomer mixtures are demonstrated.

Next we consider crystallizable stereo-regular sequences in copolymers as thermodynamic components. If the co-units are irregularily distributed, these copolymers display eutectoid crystallization with a unique correlation between chain structure and the thickness distribution of the mixed, extended-sequence micro-phases. The segregation demanded by the thermodynamics seems to take place even in semi-crystalline networks where the chains are linked as components in the network. It is then possible to describe the kinetics of thermally and strain-induced crystallization. Here, one has to combine the thermodynamics of eutectoid copolymers with the van der Waals model of real networks.

Measurements with a micro-stretch calorimeter extend substantially the analytical power of caloric measurements. In combination with X-ray investigations, a relatively consistent description of the cluster structure in semi-crystalline copolymers and networks is obtained.

Both eutectoid oligomer multi-component systems and eutectoid copolymers come relatively near to thermodynamic equilibrium. This can only be explained if the segregation of components takes place on a very local scale within thermodynamically equivalent sub-systems of finite size. These processes are strictly synchronized by the thermodynamics so as to allow them to be studied by macroscopic measurements.

INTRODUCTION

An important driving force in nature is to enforce a unique molecular conformation and configuration by a defined chemical structure. But, in synthetic polymers and copolymers, the chemical chain structure is not unique. Co-units may, for example, be randomly distributed among the chains. The question arises therefore as to the manner in which crystallization occurs in such systems, and as to how the chain and colloid structures are inter-related [1–15].

Chain ends or different co-units operate on a local level as "quasi-eutectic units". They are crystal-lattice-incompatible. Being linked in chains, these eutectic units can only be segregated during crystallization by forming extended-chain or extended-segment lamellae. These micro-phases are thermodynamically determined "primary elements" of the colloid structure. Their thicknesses is uniquely determined by the inherent mean lengths of the chains or regular sequences.

To explain our theoretical route, we will first review the thermodynamics of eutectoid oligomer multi-component systems [15]. Chain ends are squeezed out of the core of extended-chain, mixed-crystal defect layers, making mixed micro-phases inhomogeneous. The thermodynamics of such micro-phases has been developed and has revealed that the thickness of the boundaries and, hence, the excess situation in mixed micro-phases are controlled by the maximum disparity in chain length. Moreover, mixed micro-phases are only stable if this difference is not too large. Otherwise, eutectic or eutectoid crystallization occurs. The excess parameters of homologues can be related to the disparity in their chain lengths. This allows isobaric state diagrams, to be described and predicted. For systems with a broad distribution of chain length, mixed micro-phases with a maximum number of components are formed. Their thickness distribution is then well defined by the chain length distribution itself.

It is very important to note that in multi-component systems, many identical micro-phases come into existence. They are distributed throughout the volume of the system and are, therefore, exposed to different environments. Macroscopic phenomena, such as melting, are then only readily described if identical micro-phases are thermodynamically autonomous. They should show, for example, the same melting temperature, independent of their environments. Only under these circumstances do macroscopic phenomena of melting not depend on the configuration of the micro-phases. Any thermal analysis of melting relies on this fundamental symmetry.

We can now consider eutectoid copolymers, confining our treatment of copolymers to representative examples with two different, lattice-incompatible co-units. Stereo-regular chain sequences of sufficient lengths (c-sequences) are of interest. In the treatment of oligomer multi-component systems it is advantageous if c-sequences of different lengths are considered as thermodynamic components, despite their being linked in chains. This is indeed, an interesting and unconventional model. It is then clear that copolymers with a broad distribution of crystallizable sequences must be considered as eutectoid multi-component systems comprised of many homologues of different lengths. "Component-saturated", lamellar, extended-sequence mixed crystals with defect boundaries come into existence. We will demonstrate that the thermodynamically demanded

segregation of c-sequences is possible, even in networks where they are permanently linked together [16, 17]. X-ray synchrotron measurements provide additional knowledge of how clusters are developed as secondary elements of the colloid structure in eutectoid copolymers. Moreover, it is finally possible to discuss the kinetics for thermally or strain-induced crystallization [18].

It is, again, most significant that semi-crystalline copolymers seem to be composed of not too large thermodynamically equivalent sub-systems [19]. Without any long-range diffusion, equilibrium can be established within each of the sub-systems. Thus, due to the thermodynamic equivalence of the sub-systems, crystallization or melting is synchronized among all of them. Macroscopic observation reflects the local events.

In this paper, extra emphasis is given to the thermal analysis of melting and crystallization. Among other analytical methods, this method offers outstanding possibilities for characterization. Most interesting in this respect is a micro stretch-calorimeter because it provides the total energy balance during deformation which offers extra possibilities for testing our concept.

OLIGOMERS

In this section we explain the crucial steps in developing the thermodynamics of multi-component systems comprised of linear chains with a unique, stereo-regular structure. The chain ends are crystal-lattice incompatible. They are squeezed into extra layers, and lamellae are formed. We consider these lamellae as "micro-phases". The utility of this model becomes evident in describing mixed, extended-chain crystals. Distorted layers are developed so that these micro-phases no longer have a homogeneous structure. To define such lamellae as cooperative units of a colloid system is a significant extension of the classical thermodynamics of solid solutions, because this provides the "primary, thermodynamically defined, finite sized elements" of the colloid structure [15, 20–22]. It is clear that melting in oligomer or copolymer systems is dramatically changed if folded chain crystallization takes place [1, 23–28].

Single component systems

We must explain the origination of the chain-length dependence of the melting points of extended-chain crystals in an oligomer single-component system [1, 21, 29]. To this end, the chain-length parameter is defined as the number of periodic units y. The thickness of the sub-lamellae is therefore

uniquely related to y. The excess free enthalpy per chain end is defined by $\sigma_e > 0$.

For even or odd linear oligomer homologues, the melting temperature T_y is then described by the Flory–Vrij equation [30]

$$T_y = T_m \frac{1 - 2\sigma_e(T)/\Delta h(T)y}{1 + [RT/\Delta h(T)y]\ln(y)} \quad (1)$$

where $\Delta h(T)$ is the molar melting enthalpy per unit, which depends on temperature according to

$$\Delta h(T) = \Delta h(T_m) - \Delta c(T_m - T) \quad (2)$$

where T_m is the asymptotic melting temperature of the extended-chain crystal of "infinite" thickness, and Δc is the specific molar heat capacity of the periodic unit. The numerator is the Thomson relationship according to which T_y is increasingly depressed as the chains become shorter.

From the representation of experimental data as shown in Fig. 1 [15, 21, 22, 31, 32], it is clear that the molar free enthalpy of melting of not too short oligomer homologues can be related to the periodic unit (CH_2 unit). Moreover, the excess enthalpy of the chain ends σ_e does not depend on chain length. The ratio $2\sigma_e(T)/\Delta h(T)$ is also constant. Hence, the excess properties in the chain-end layers must have relatively local origins. If we ignore the effects due to different lattice symmetries, this explains why the melting temperatures of homologues are unique functions of the chain length parameter y.

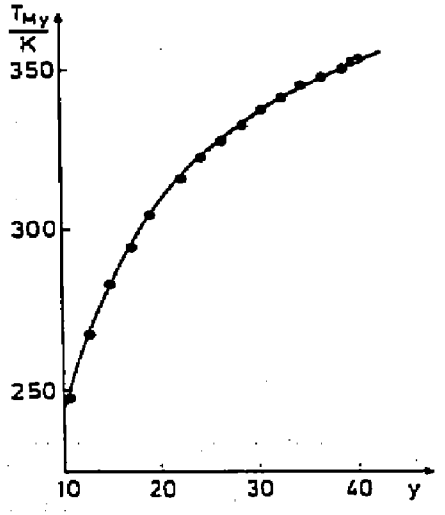

Fig. 1. Melting temperatures of even n-paraffins as a function of the chain-length y [15]. The solid line is computed with the aid of eqn. (1): $T_m = 415$ K, $\Delta h = 4046$ J mol^{-1}, $2\sigma_e/\Delta h = 2.11$, $\Delta c = 1.4$ J mol^{-1} K^{-1}.

The micro-phase concept

The extended chain crystal is comprised of densely packed lamellar subunits of identical thickness. These "primary structure elements" are now considered as autonomous micro-phases [15]. They are thermodynamically equivalent. Each one has, for example, the same melting temperature. Isobaric melting of the whole assembly of lamellae occurs at constant T_s so as to yield the same macroscopic features as for classical phase transitions in a single component system [33, 34]. Coexistence between the melt and each of the sub-systems is immaterial (neutral).

Mixed oligomer systems

If identical micro-phases are equivalent, it follows that the topology of the state diagrams for micro-phase systems with more components must be the same as in classical thermodynamics. This symmetry is very important for interpreting macroscopic measurements in multi-component systems.

Systems comprised of chains of different lengths are mixtures [15], in which the chains of different lengths are the components. Mixed extended-chain micro-phases (EMC) have a structure as illustrated in Fig. 2. Due to the mismatch in chain lengths, more or less distorted layers come into existence. It is now very important to assume that the whole EMC can be treated as an "inhomogeneous micro-phase". It is also assumed that internal equilibrium is established within these layers. Defect properties can then formally be described without explicitly indicating where the defects are located. Yet, if the defect structure in the boundaries is thermodynamically optimized, it should unqiuely depend on the disparity in chains lengths. A detailed description should therefore provide information on the mean structure in the defect boundaries themselves.

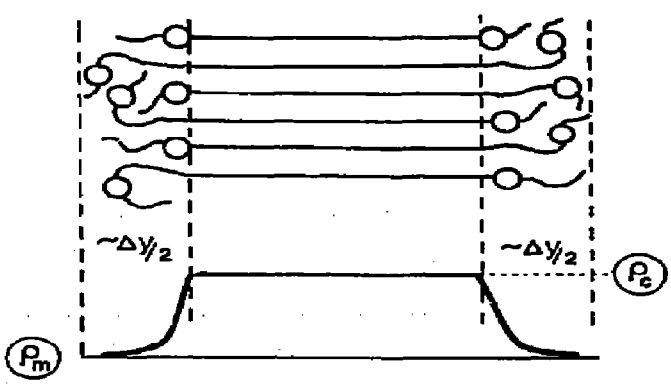

Fig. 2. Sketch of an extended-chain mixed micro-phase (EMC). Within the defect boundaries the average density ρ falls below that in the crystal core. In the outer layers, ρ is deduced to be smaller than the mean density in the melt.

Due to the equivalence of micro-phases, classical thermodynamics is again only modified by finite size effects. For coexistence of mixed micro-phases in oligomer multi-component systems, the chemical potentials of the components within each of the micro-phases (the melt included) must be identical. For chains of length y_k in the mixed micro-phase α, $\mu_{y_k}^{(\alpha)}$, we obtain

$$\mu_{y_k}^{\alpha} = \mu_{0y_k}^{\alpha} + RT\ln(\varphi_{y_k}^{\alpha}) + g_{ex,y_k}^{\alpha}$$

$$\mu_{0y_k}^{c} = y_k h_0^{c} + 2\sigma_e - T(y_k s_0^{c}) \tag{3}$$

$$\mu_{0y_k}^{m} = y_k h_0^{m} - T(y_k s_0^{m})$$

where $\mu_{0y_k}^{\alpha}(T, p)$ is the standard potential of the pure phase α at the pressure p and the temperature T. The molar fraction $\varphi_{y_k}^{\alpha}$ is written as

$$\varphi_{y_k}^{\alpha} = \frac{n_{y_k}^{\alpha} y_k}{\sum n_{y_i}^{\alpha} y_i} \qquad \sum \varphi_{y_k}^{\alpha} = 1 \tag{4}$$

where $n_{y_k}^{\alpha}$ is the mole number of chains of length y_k. The surface free enthalpy correction $2\sigma_e > 0$ is included in $\mu_{0y_k}^{c}$. g_{ex,y_k}^{c} is the partial molar excess free enthalpy arising from defects in the boundaries. The partial molar free excess enthalpy may be written formally as [34–36]

$$g_{ex,k}^{\alpha} = \left(\frac{\partial g_{ex}^{\alpha}}{\partial n_k^{\alpha}}\right)_{T,p} = \sum_{\substack{i=1 \\ i \neq k}}^{N} A_{ik}^{\alpha} x_i^{\alpha}(1 - x_k^{\alpha}) - \tfrac{1}{2} \sum_{i>1}^{N} A_{1,i}^{\alpha} x_1^{\alpha} x_i^{\alpha} \tag{5}$$

where N is the number of components. Only second virial coefficients A_{ik}^{α} are considered. This is important if the excess free enthalpy is dominated by pair interactions.

In extended-chain mixed micro-phases, the cross-section of chains of different length is practically identical. The mixing entropy in the solid solutions is therefore correctly formulated in terms of the mole fractions $x_{y_k}^{c}$

$$x_{y_k}^{c} = \frac{n_{y_k}^{c}}{\sum n_{y_k}^{c}} \qquad \sum x_{y_i}^{c} = 1 \tag{6}$$

If we neglect excess properties in the melt, micro-phase equilibrium is achieved if "chemical equilibrium" is established

$$\mu_{y_k}^{c} = \mu_{0y_k}^{c} + RT\ln(x_{y_k}^{c}) + \sum_{k>i} A_{ik}^{c} x_k^{c}(1 - x_k^{c}) - \tfrac{1}{2} \sum_{k=1} A_{1,i}^{c} x_1^{c} x_i^{c}$$

$$= \mu_{y_k}^{m} = \mu_{0y_k}^{m} + RT\ln(\varphi_{y_k}^{m}) \tag{7}$$

for all $N - 1$ components.

The excess parameters

From a description of the binary isobaric state diagrams of *n*-alkanes, the following empirical relationship was deduced

$$A^{c}_{ik} = A_0 \frac{\Delta y_{ik}}{\langle y^c \rangle} \qquad \Delta y_{ik} = |y_i - y_k| \tag{8}$$

The excess free enthalpy is simply proportional to the disparity in chain length $\Delta y = y_i\ y_k (y_i > y_k)$ and inversely proportional to the mean chain length in the crystalline micro-phases $\langle y^c \rangle$

$$\frac{1}{\langle y^c \rangle} = \sum \frac{y_k}{\varphi^{c}_{y_k}} \tag{9}$$

The parameter A_0 was found to depend somewhat on the number of components in the solid solution. Yet, on increasing this number, A_0 goes to an asymptotic value. Equation (8) verifies that the boundaries of EMCs are in equilibrium. The excess situation is controlled by the chemical structure of the components. The whole lamella represents an inhomogeneous micro-phase in the strict thermodynamic sense. It constitutes a most important primary element of the colloid structure in an oligomeric multi-component system with extended-chain mixed crystals.

The component-saturated mixed micro-phase

Multi-component systems of equimolar composition are considered as a special case. We want to know whether the solubility in EMCs is in principle limited ($N = N_{max}$). This would have the consequence that oligomer multi-component systems with extended-chain crystals would show eutectoid crystallization.

In this case, the molar fractions have the same value

$$x^{c}_{k} = \frac{1}{N} \tag{10}$$

Together with the relationship obtained from binary systems

$$A_{ik} = \langle A \rangle \frac{\Delta y_{ik}}{\langle y^c \rangle} \tag{11}$$

the Gibbs free energy

$$G^c = \sum_i g^{c}_{0i} n^{c}_{i} + RT \sum_i n^{c}_{i} \ln x^{c}_{i} + \sum_{i} \sum_{\substack{k \\ i<k}} A^{c}_{ik} x^{c}_{i} x^{c}_{k} \tag{12}$$

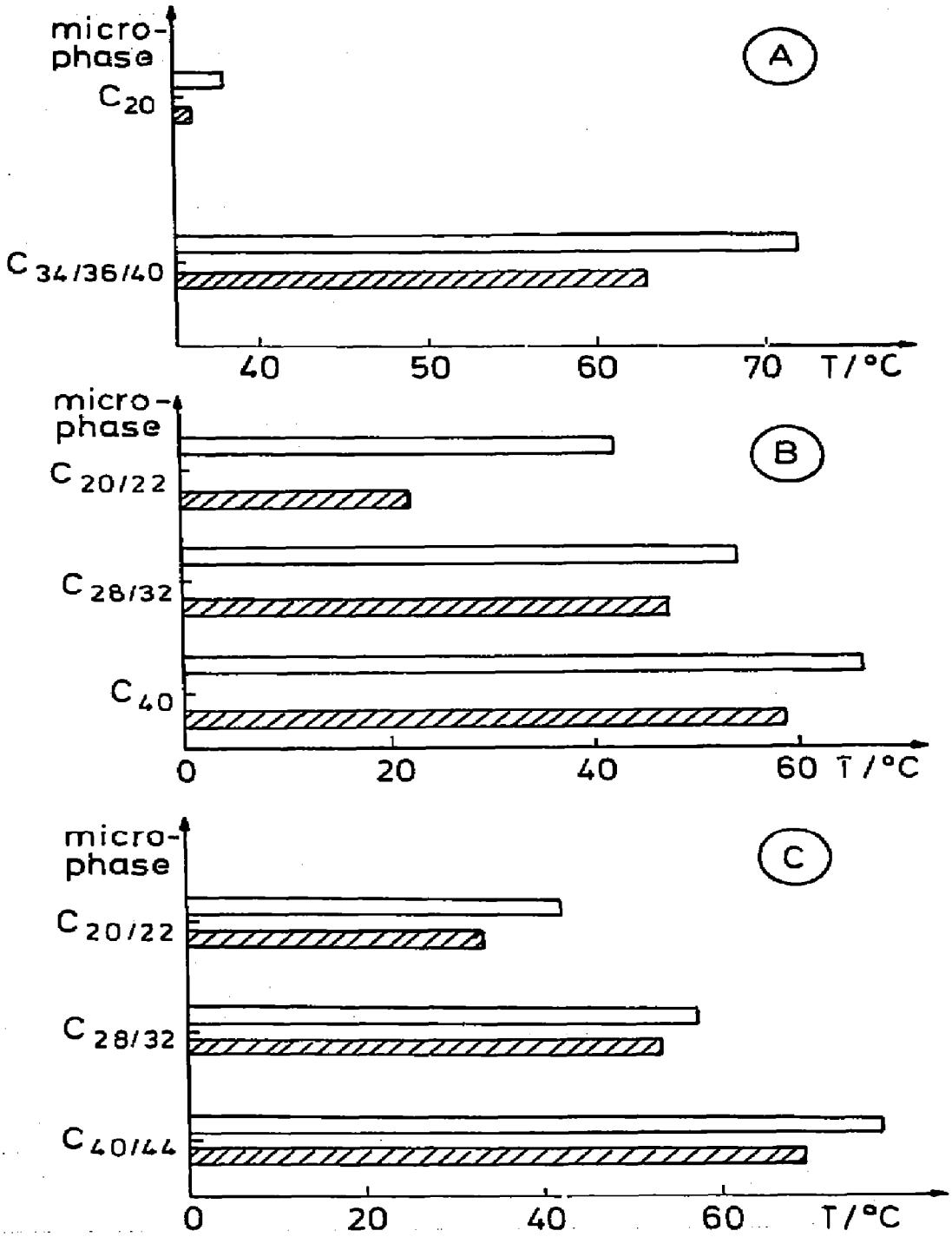

Fig. 3. Liquidus temperatures of EMCs of the types indicated [15]. For example, $C_{20/22}$ is a binary EMC consisting of chains of lengths $y_1 = 20$ and $y_2 = 22$. The hatched bars represent predicted data; the unfilled bars give the experimental data. In the synchrotron X-ray patterns versus temperature different sets of diffraction peaks are indicated with the symbols *a*, *b* and *c*. The liquidus temperatures at which the last EMCs of a special type disappear are attached to the first-order peak.

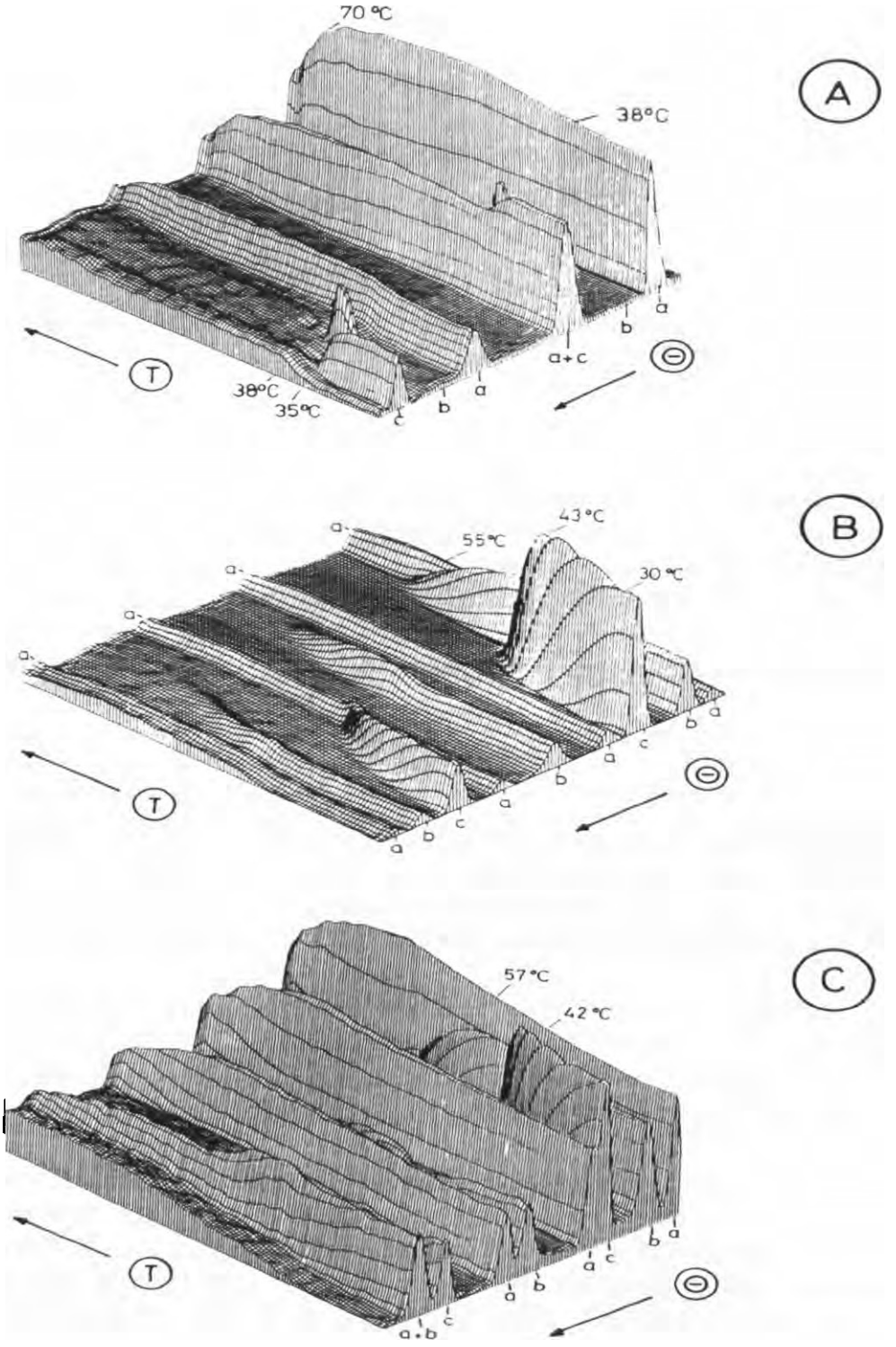

Fig. 3 (continued).

is found to be equal to

$$G^e = \sum_i n_i^e \left[G_{0i}^e - RT \ln N + \frac{1}{N^2} \frac{\langle A^e \rangle}{\langle y^e \rangle} \sum_i (N - i + 1)(N - i) \right] \tag{13}$$

The free enthalpy is a minimum for the maximum number of equimolar components N_{max}

$$N_{max} = 6 \frac{RT}{\langle A^e \rangle} \langle y^e \rangle = \Delta y \tag{14}$$

so that the maximum disparity in chain lengths in a component-saturated EMC may be written as

$$\Delta y = M \langle y^e \rangle \qquad M = 6 \frac{RT}{\langle A^e \rangle} \tag{15}$$

Hence, component-saturated EMCs should exist. Even the maximum mixing entropy in equimolar ideal mixtures is overpowered by the excess enthalpy if the number of components exceeds the value given in eqn. (14). This result agrees with the relationship as deduced from many experiments, see eqn. (16) below. Hence, in defect layers, segmental pair interaction is dominant, making excess quantities a unique function of disparities in chain length.

Results and discussion

Using the above equations, it is possible to calculate isobaric state diagrams of oligomer multi-component systems [15]. The number and types of stable solid solutions are correctly predicted, see Fig. 3. The reproduction of desmeared DSC traces demonstrates the quality of our description, Fig. 4.

Solid solutions are formed only if the maximum disparity in chain lengths is lower than about 20–30% of the mean chain length $\langle y^e \rangle$. Hence, compatibility in the solid solutions of oligomers is strictly limited, whereby the maximum disparity in the chain length obeys the relationship defined by eqn. (8).

It is significant that real, mixed, extended-chain micro-phases fulfil the coexistence conditions of eutectoid crystallization. In the melting range, each type of EMC shows a different composition at each temperature. The mass fractions are adjusted according to the lever rule in the hyper-space of a eutectoid multi-component system. This is verified in the comparison of model calculations with experiments, as shown in Fig. 5 [36].

Another interesting observation is shown in Fig. 6. On cooling, two new, different five-component mixed micro-phases are formed. In the synchrotron X-ray pattern, this is indicated by the splitting into two sets of peaks. Micro-phase separation occurs in good accord with thermodynamics.

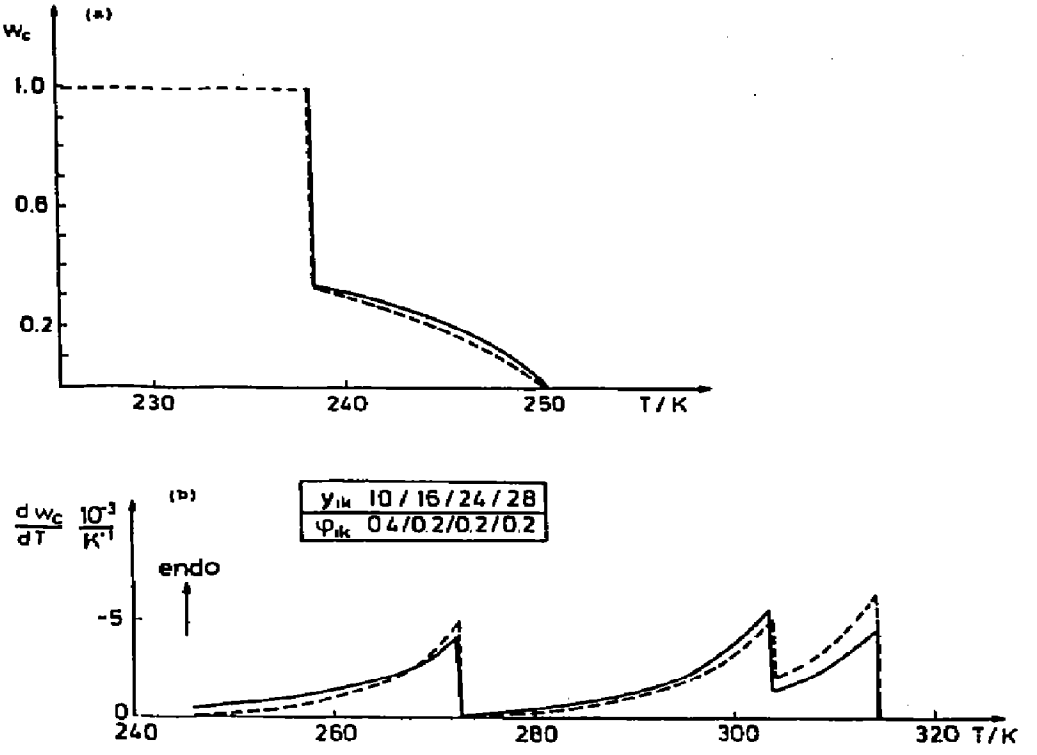

Fig. 4. (a) The molar degree of crystallinity w_c plotted against temperature for the eutectic binary n-alkane mixture composed of chains of lengths $y_1 = 10$ and $y_2 = 12$ for a volume fraction of $\varphi_{10} = 0.496$. The dotted line is theoretical [15]. (b) Plot of dw_c/dT for a four-component n-alkane mixture (—, desmeared experimental; – – –, theoretical) composed of chains of lengths $y_1 = 10$, $\varphi_{10} = 0.4$; $y_2 = 16$, $\varphi_{16} = 0.2$; $y_3 = 24$, $\varphi_{24} = 0.2$; $y_4 = 28$, $\varphi_{28} = 0.2$ [15].

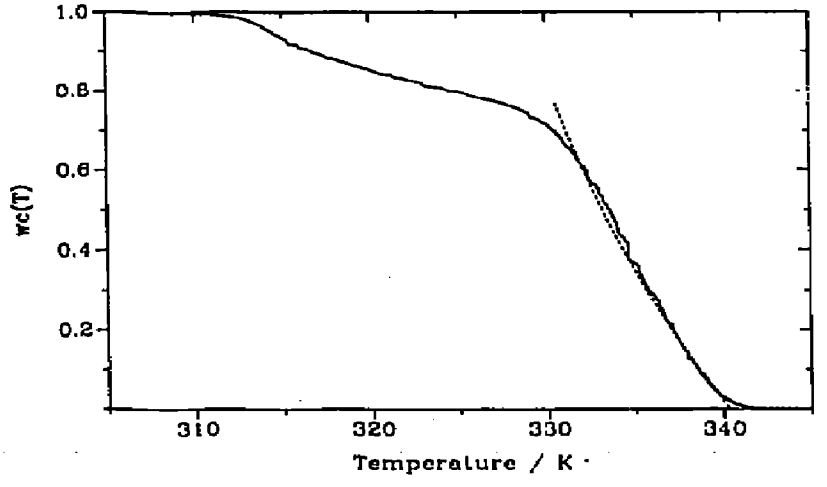

Fig. 5. Molar degree of crystallinity plotted against temperature for an n-alkane mixture composed of seven components of identical mass fraction (even y ranging from $y_1 = 24$ to $y_7 = 40$). The solid line represents the computed results for hexagonal rotator-phase crystals [36].

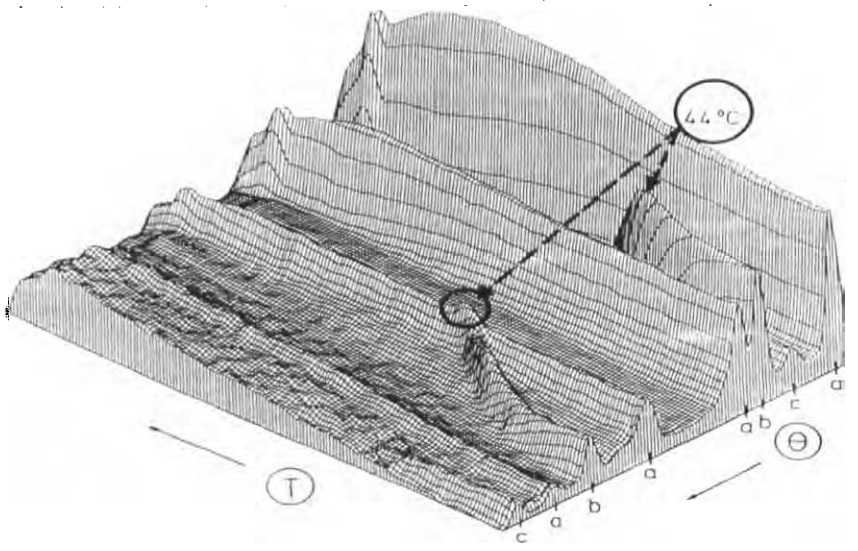

Fig. 6. Synchrotron SAXS pattern of a five-component n-alkane mixture with a five-component solid solution, plotted against temperature [15]. On cooling, two new peaks appear at $T < 44$°C. Two five-component EMCs with different composition, as demanded by thermodynamics, appear, forming stacks with more than eight identical lamellae within periods of time shorter than 15 s.

Micro-phase transitions in real oligomer more-component systems must be strictly synchronized so as to the same topology as in classical thermodynamics. Even in the crystallized five-component system, phase separation is achieved within a very short period of time: in the example described, below 10 s.

Three to four orders can only be observed in the X-ray pattern (Figs. 3 and 6) if more than about eight identical lamellae are packed together. Hence, EMCs of the same thickness are clustered. This is possibly due to the strongest interaction being across defect layers of pairs of identical EMCs.

It appears that the cluster structure does not influence state diagrams to measurable extents. Moreover to have calculated the correctly predicted complicated state diagrams in more-component systems supports the model of an autonomous micro-phase.

Defect saturation

We proceed now to eutectoid multi-component systems with a very broad chain-length distribution, $\phi(y)$ [15]. Most significant is that the solubility in EMCs must be limited to a thermodynamically defined maximum disparity in chain lengths ("component-saturation" of EMCs) (see The component-saturated mixed micro-phase, see p. 119)

$$\Delta y = A\langle y^c \rangle \tag{16}$$

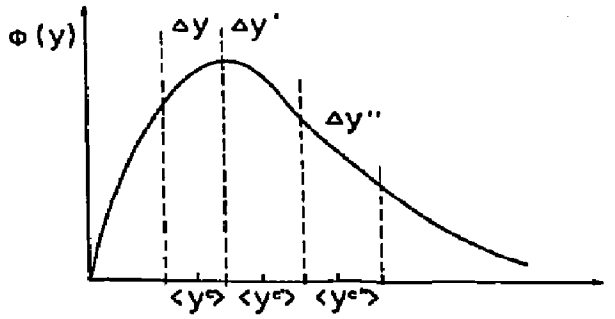

Fig. 7. A diagram to illustrate that molar mass distribution (solid line) and crystal-thickness distribution must be uniquely interrelated. An EMC of mean thickness $\langle y^c \rangle$ includes chains of lengths $\langle y^c \rangle - \Delta y/2 \leq y \leq \langle y^c \rangle + \Delta y/2$.

If Δy is sufficiently small, the thickness distribution of EMCs Ψ ($\langle y^c \rangle$) is uniquely determined by the chain length distribution $\phi(y)$

$$\phi(y) \equiv \psi(\langle y^c \rangle) \tag{17}$$

This is illustrated in Fig. 7.

The melting process

Two typical factors characterize melting and crystallization in the oligomer multi-component systems. Firstly, the free surface enthalpy, together with the excess energies, depress the melting temperature of EMCs. The smaller the crystal core (as in eqn. (1) [37–39]), the larger the depression. However, melting also depends on the composition of the multi-component melt (see eqn. (22)). Both effects together lead to the characteristic that melting runs selectively and consecutively, beginning with EMCs of smallest thickness at the lowest temperature, followed by the new fraction of the smallest micro-phases (Fig. 8). It is due to this

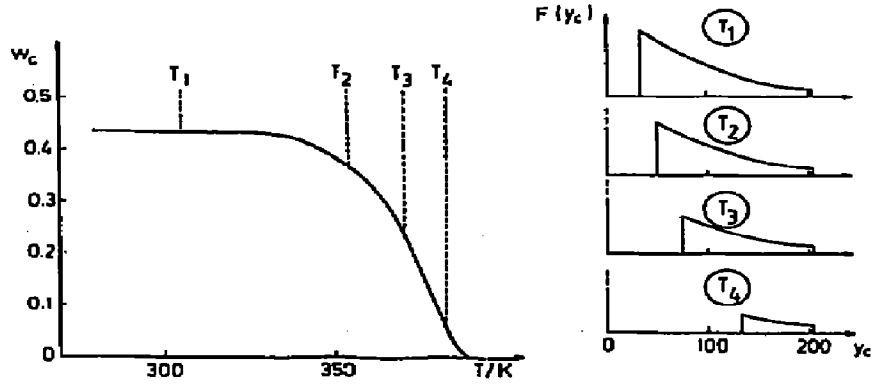

Fig. 8. Crystallinity w_c of a eutectoid system with component-saturated microphases plotted against temperature. On the right, it is shown that the width of the micro-phase thickness distribution decreases due to selective and consecutive melting.

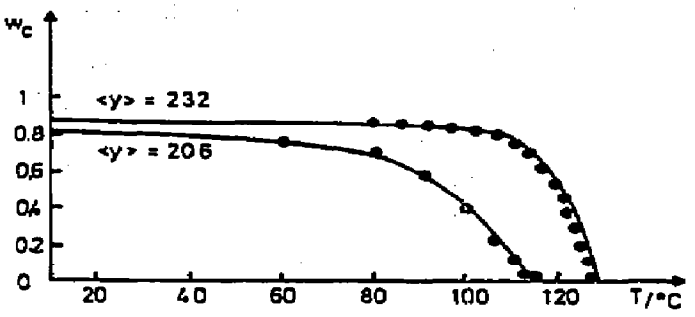

Fig. 9. The molar degree of crystallinity for fractions of linear polyethylene with two different mean chain lengths ($\langle y \rangle = 206$, $\langle y \rangle = 232$) plotted against temperature. Because of the defect layers of the EMCs, the equilibrium condition $w_{c\,max}^{(1)} < w_c^{(2)} < 1$ results.

consecutive process that the melting curves are uniquely determined by the thickness distribution of EMCs Ψ ($\langle y^c \rangle$). This is equivalent to saying that the shape of every DSC curve is a copy of the differential chain-length distribution (eqn. (17)).

Here, we show the melting curves of two fractions of polyethylene (Fig. 9). In both cases, even the longest chains are short enough such that folded-chain crystallization does not occur. The solid lines were computed using Tung functions. Both curves deviate clearly from each other. The $\phi(y)$ values are, however, not very different. This demonstrates the accuracy with which chain-length distributions can be deduced from DSC traces of multi-component oligomer systems. The results are found to be in good accord with gel chromatographic measurements [40].

It is clear that not too large equivalent sub-systems must exist so as give the whole system a real chance of approaching eutectoid multi-micro-phase equilibrium states. This seems to be the principle feature characterizing such systems.

Folded-chain lamellae

A folded chain crystal of fold height y_f may include very different chain lengths. These chains must all satisfy the condition $y > 2y_f$ [23–28, 39–45]. Yet, due to fold loops, most of the crystallized stems can no longer be freely exchanged. Hence, folded chain crystals cannot behave like mixed extended-chain micro-phases. The configuration of folded chain segments is de facto frozen in and can only be modified by a cooperative reorganization within larger complexes. Moreover, the fold height itself depends on the crystallization kinetics.

It is interesting that the analysis of the melting of waxes [40, 46] with a broad chain-length distribution allows crystallization in multi-component oligomer systems, where folded chain crystals and EMCs are both formed,

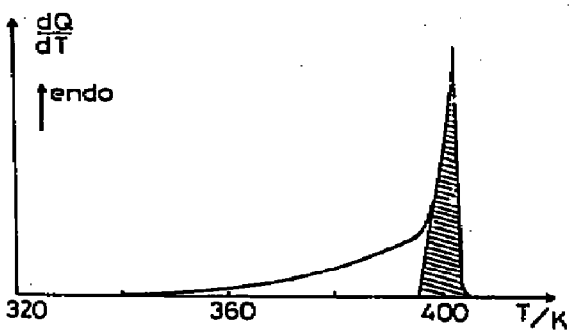

Fig. 10. DSC trace of melt-crystallized polyethylene wax (PE130) for a heating rate of 0.5 K min^{-1}. The hatched area is associated with the melting of folded-chain crystals [36, 46].

to be classified. The DSC peak at highest temperatures in Fig. 10 belongs to folded chain crystals. Folded chain crystals are formed in the high-temperature regime, the range in which, under equilibrium conditions EMCs of greatest thickness are the absolute stable micro-phases. EMCs are, however, formed in the temperature range $T < T_f$. Despite the presence of folded chain crystals, the analysis of their broad melting processes is possible so as to obtain their thickness distribution.

Folded chain crystals are in principle distinct from EMCs [34]. Spherulites are often observed. Within each spherulite a framework of bundles is formed, each comprising more than ten folded-chain lamellae packed densely together (Fig. 11). Clearly, "eutectic-like nucleation and growth" of folded chain crystals characterizes the features of spherulites or other super-structure elements. Cooling down to lower temperatures, EMCs fill continuously the space between the folded chain crystals. Because of the continuous adjusting of composition and mass fraction, rearrangement of their configuration is possible. For this reason the final colloid structure in waxes is complex and no longer simply related to the chain-length distribution.

The conclusion is clear: the chemical structure controls the primary elements of the colloid structure only if folded-chain crystallization does not occur.

COPOLYMERS

If they are composed of at least two lattice-incompatible co-units, the crystallization of copolymers should obey the same thermodynamic principles as oligomer systems [11, 15]. A new aspect is that all the components are linked in chains. If the molar masses are large, crystallization-induced segregation of special chain segments might become hindered. For this reason, it is crucial that smaller thermodynamically equivalent sub-systems come in existence. The size of the sub-systems might depend on how the units are distributed across the chains. Their

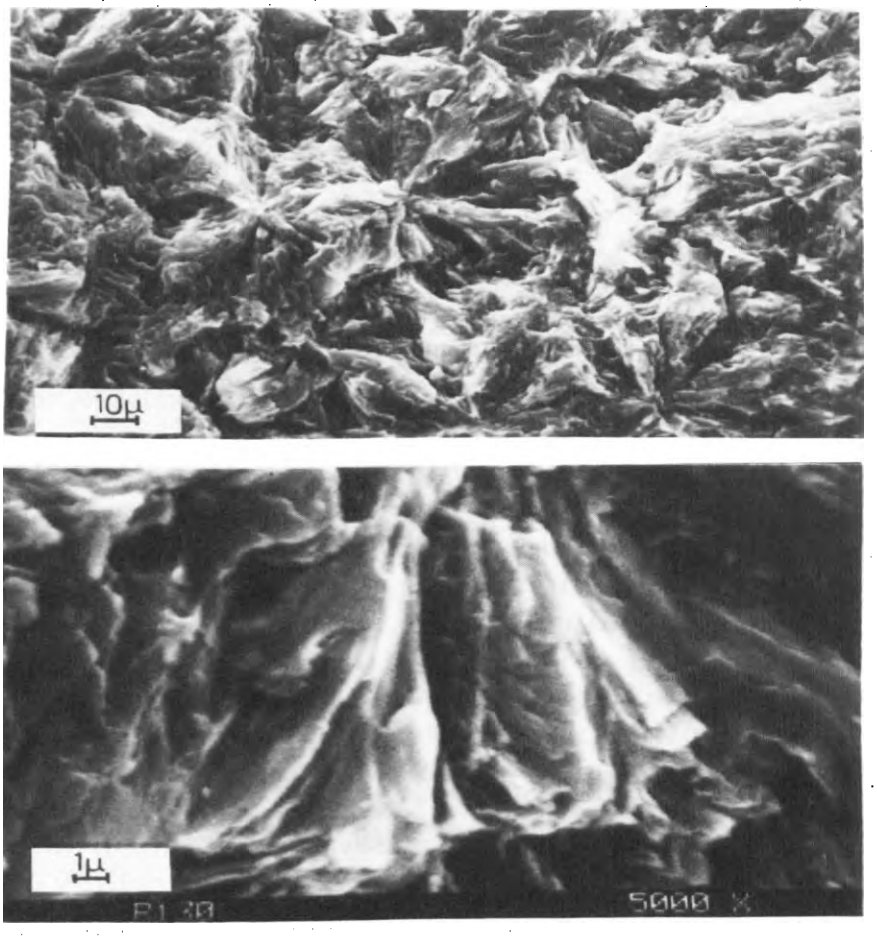

A

B

Fig. 11. EM photographs of melt-crystallized PE130.

existence should allow the segregation of special chain segments, as demanded by thermodynamics. This is verified by describing melting and crystallization in macromolecular networks. Despite the chains being linked in a network, a surprisingly satisfactory description that includes crystallization kinetics can be obtained.

The first theory was derived by Flory [11]. One of its severe shortcomings is that the maximum crystallinity is not correctly predicted [3, 47]. While Flory [11] considered strict exclusion of the non-crystallizable units (nc-units) from the crystal lattice, many authors suggested reasons for assuming that at least some of the nc-units are included in the solid micro-phases [25, 48–55]. This was discussed in terms of a two-phase model. But, it is evident that inhomogeneous micro-phases "incorporate" a remarkable number of nc-units. The crystal core properties are likely to be cooperatively interrelated with the situation at the boundaries. We therefore retain the model of non-homogeneous micro-phases which appears to be much more satisfactory.

The chain-structure

In the simplest case, crystallizable linear copolymers are composed of two lattice-incompatible units (quasi-eutectic co-units), such as, for example CH_2 units and short-chain branchings in low density polyethylene. We define the molar fraction of the crystallizable co-units x_c by

$$x_c = \frac{n_c}{n_c + n_{nc}} \qquad x_c + x_{nc} = 1 \tag{18}$$

For two different co-units the unit having the smallest concentration is conveniently called the "non-crystallizable unit" ("nc-unit"); n_{nc} represents the mole number of these units while n_c is the mole number of "crystallizable units" (c-units). If the concentration of nc-units is small, a length distribution of sequences of c-units (c-sequences) is built up [3, 15, 56]. The length of any c-sequence should be defined by the number of periodic units linked into it.

Because the c-sequences are assumed to be stereo-regular, crystallization must be controlled by their length distribution $C(y)$. In some cases, $C(y)$ can be expressed analytically. For a random distribution, the normalized molar fraction of c-sequences of length y is equal to

$$C(y) \equiv x_y = x_{nc}^2 x_c^{y-1} \qquad \sum_{y=1}^{\infty} x_y = 1 \tag{19}$$

Here, crystallization should only be possible if the molar fraction of nc-units x_{nc} is smaller than 0.13–0.15. If crystallization is observed above these limits, it might be that the c-sequence lengths are not randomly distributed [57].

Extended c-sequence mixed crystals (EMSC)

The treatment of eutectoid oligomer systems is also applicable here if c-sequences of different length are defined as components, despite their being linked in chains. These pseudo-particles are not autonomous. Constraints might become so important that c-sequences of different lengths cannot be "correctly" segregated.

For copolymers with a broad c-sequence length distribution $C(y)$, extended c-sequence mixed crystals (EMSCs) should be formed [14, 15]. A sketch of an EMSC is shown in Fig. 12. Hence, copolymers should undergo eutectoid crystallization. The "component-saturated" EMSCs are characterized by a maximum disparity of c-sequences Δy, which was found to be defined by [15, 58]

$$\Delta y = A\langle y \rangle + B \qquad B = B_1 \frac{x_c}{x_{nc}} + B_2 \tag{20}$$

Because B has large values, solubility in the EMSCs is very much greater

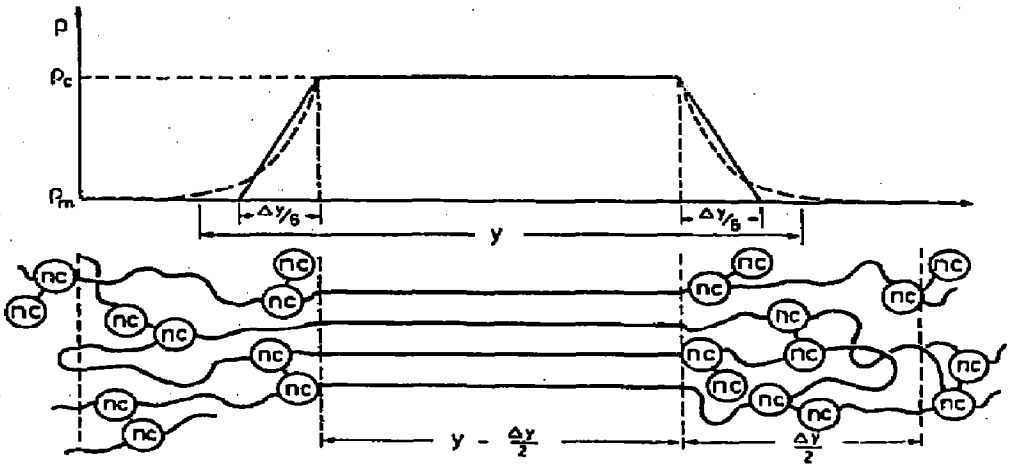

Fig. 12. A two-dimensional sketch of an EMSC showing the inhomogeneous distribution of nc-units (in the present case junctions of a permanent network). In the outer boundaries, the density decreases rapidly to the value the melt: y represents the mean length of c-sequences in the micro-phase; Δy is the maximum disparity of chian lengths.

than in oligomer mixed micro-phases (eqn. (8)). In small EMSCs, the excess energies should be very much reduced

$$\Delta y_{\text{oligomers}} = A\langle y\rangle \ll A\langle y\rangle + B \tag{21}$$

For many different copolymers also displaying different $C(y)$ values, the parameter $b(x_{nc})$ falls on a master curve (Fig. 13). For linear copolymers, the defect structure in the boundaries seems to be typical and universal, representing an equilibrium property. Hence, it is fully justifiable to treat EMSCs as inhomogeneous micro-phases in the strict thermodynamic sense.

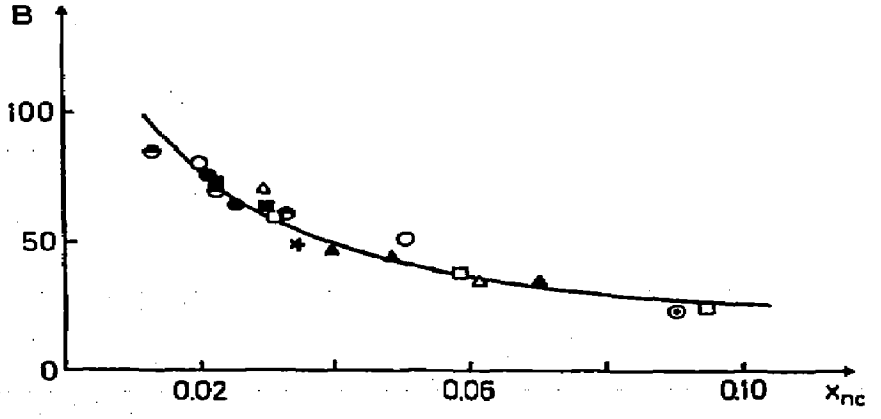

Fig. 13. $B(x_{nc})$ values of different copolymers, according to ref. 58: ★, random copolymers of ethylene; ○, vicinal chlorinated polyethylene; ⊙, poly-oxy-methylene copolymers; □, ethylene-tetrafluoro-ethylene copolymers; ■, bipolymers; △, terpolymers; ▲, networks.

A complete understanding of the parameter B in eqn. (20) has not yet been achieved. The most plausible explanation is to consider B as an internal parameter that describes the limits of arranging short-chain segments and nc-units so as to minimize the excess free enthalpy in the boundaries of EMSCs.

Coexistence

Because we know the maximum disparity of chain lengths for each EMSC, Δy, the coexistence conditions can be deduced by equalling the chemical potentials of only one component. This suggests that c-sequences which have the same length as the mean c-sequence lengths within the EMSC ($\langle y^c \rangle \equiv y$) can be selected.

For the c-sequences $\langle y^c \rangle \equiv y(T)$, the temperature of coexistence T_y is written as

$$T_{y(T)} = T_m \frac{1 - 2\sigma_e/N_1}{N_2}$$

$$N_1 = \Delta h(y(T) - \Delta y/3)$$

$$N_2 = 1 + \frac{RT}{N_1}\left\{\ln\left[\frac{y(T)}{(\Delta y/2 + 1)}\right] - \ln\left(\frac{x_y^m}{x_y^c}\right) - \frac{y(T) - 1}{2}\chi^m\right\}$$

$$x_y^c = \frac{C(y(T))}{2N_3} \qquad N_3 = \sum_{y_k = y(T) - \Delta y/2}^{y(T) + \Delta y/2} C(y_k) \tag{22}$$

$$x_y^m = \frac{C(y(T))}{2N_4} \qquad N_4 = \sum_{y_k = 1}^{y(T) - 1} C(y_k)$$

where χ''' is the Flory–Huggins parameter per unit in the melt. The excess parameter term in eqn. (22) is an approximation for systems with a very broad $C(y)$. For the same reasons that were applied to eutectoid oligomer systems, the melting of EMSCs should run selectively and consecutively. The thickness of the smallest EMSCs stable at $T_{y(T)}$ is $y(T)$. The coexisting temperature of these EMSCs depends on the mole fraction in the multi-component melt $x_y^m(T)$ [14]. The influence of the mixing entropy in the non-crystallized regions is inversely proportinal to x_y^c because EMSCs are solid solutions ($-R \ln(x_y^m/x_y^c)$); x_y^c is a unique function of the maximum disparity of the c-sequence lengths Δy (eqn. (22)).

Now we justify using the molar fraction $x_y^m(T)$ in eqn. (22) instead of the volume fraction φ_y^m [14]. Because the c-sequences are linked in chains, any exchange is necessarily accompanied by a cooperative exchange of a number of next-neighboured c-sequences. If the nc-units are randomly distributed, we should find c-sequences of each length as next neighbours. On average, all c-sequences should therefore be treated as quasi-equally-sized components that are, nevertheless, distinguishable. Every deviation

from this approach simply modifies the actual value of the excess parameter χ^m.

Extensive quantities

To interpret experiments, we have to know the molar degree of crystallinity $w_c(T)$

$$w_c(T) = \frac{\sum_{y_i=y(T)}^{\infty} (y_i - \Delta y/3)C(y_i)}{\sum_{y_i=1}^{\infty} y_i C(y_i)} \tag{23}$$

which gives the total fraction of EMSCs coexisting with the multicomponent melt. Because $w_c(T)$ is a unqiue function of temperature, the temperature coefficient of the melting enthalpy is derived to be given by

$$\frac{d\Delta h^*}{dT} = -\frac{dw_c}{dT} = -\left(\frac{dw_c}{dy(T)}\right)\frac{dy(T)}{dT}$$
$$\Delta h^*(T) = \frac{\Delta h(T)}{\Delta h_{max}(T)} = \frac{h^m(T) - h(T)}{h^m(T) - h^c(T)} \tag{24}$$

This relationship allows the c-sequence length distribution $C(y > y_{min})$ to be deduced from an analysis of DSC traces; y_{min} is the absolute minimum thickness of EMS that determines the maximum degree of crystallinity as well as the lowest melting temperature.

The complete set of parameters characterizing the copolymer system is collected in Table 1. The bold parameters are known from investigations of homopolymers. Because there is a universal relationship for Δy (eqn. (20)), copolymers can be characterized by the three parameters x_c, $C(y)$ and χ^m, only.

Solubility in EMSCs

To estimate the degrees of segregation of c-sequences, let us define the solubility parameter s

$$s = \frac{\Delta y}{y(T) - 1} \tag{25}$$

where s is related to the width of chain lengths in the melt given by

TABLE 1

The set of parameters

x_c, $C(y)$; $y(T)$, T_m, $\Delta h(T_m)$, Δc, σ_e, A, B_1, B_2, χ^m

TABLE 2

Solubility s: $y_k = 17.5$; $A = 0.3$; $B = 50$

y/units	20	62	75	100	125	150	200	250	500
s/%	1	1	0.87	0.70	0.60	0.53	0.45	0.40	0.3

$y(T) - 1$, and is equal to unity if all c-sequences of different lengths in the melt can be built in an EMSC. Table 2 shows that this occurs for EMScs in the region of thickness $y < 62$. Very local rearrangements of c-sequences, at least small nematic shifts, are sufficient to form the small EMSCs, (see the data columns 5–8 in Table 8, discussed below). For very small EMSCs, there is no longer a crystal core (Fig. 14). The necessity of introducing the model of an inhomogeneous micro-phase is clear: a two-phase model is not adequate for describing largely distorted micro-phases as depicted in Fig. 14. With increasing thickness $y > 62$, the relative solubility of EMSCs approaches values as deduced for linear n-alkanes (0.2–0.35). Segregation of c-sequences of different lengths becomes increasingly important.

Comparisons with experiments

For a random copolymer, the molar degree of crystallinity $w_c(T)$ is given by [14, 15]

$$w_c(T) = (1 - A/3)x_y^{y(T)-1}[(y - y_k)x_{nc} + x_c]$$
$$y_k = B/(3 - A) \tag{26}$$

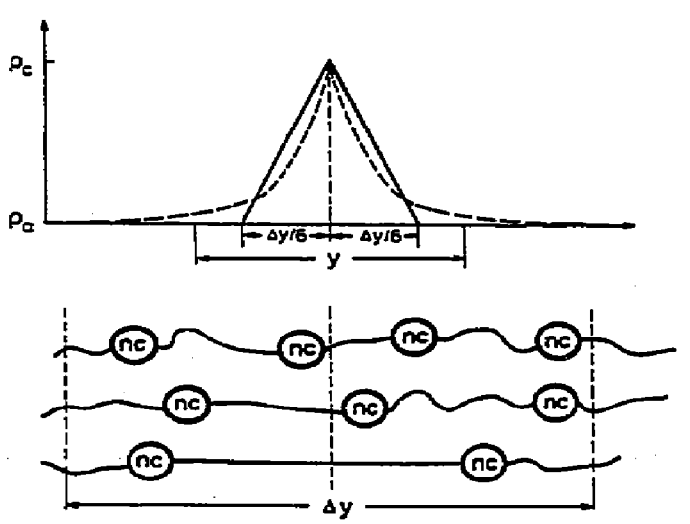

Fig. 14. Sketch of a degenerated EMSC that no longer shows a core with a well-ordered lattice.

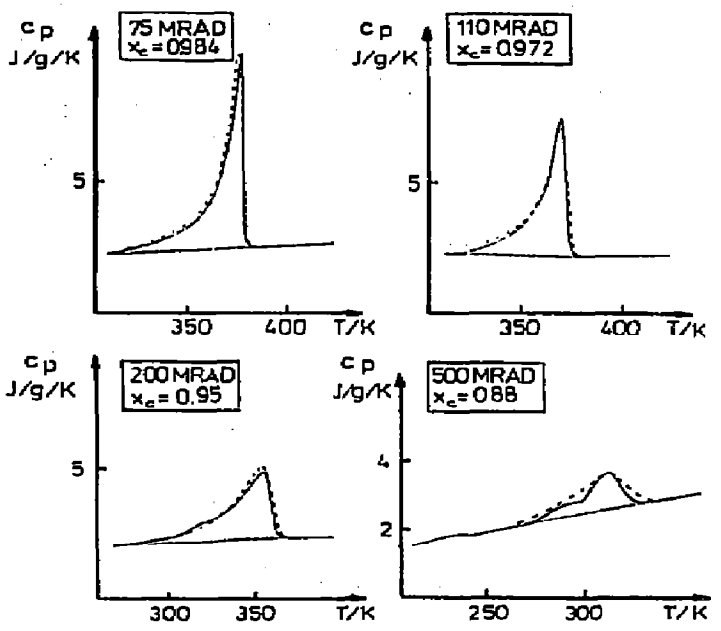

Fig. 15. DSC traces of polyethylene networks crosslinked in the melt. The dotted lines are theoretical, for parameters, see Table 3 [16].

For polyethylene radiation-crosslinked in the melt, one expects a random CH_2 sequence length distribution. By using $C(y)$ as in eqn. (19), DSC curves of polyethylene networks can reasonably be fitted (Fig. 15) [16, 51]. Because $C(y)$ is known, the only free parameters were the effective concentration of junctions (x_{nc}) and the interaction parameter per unit (χ^m)

What is striking is that the whole transition enthalpy Δh_{exp} is fairly well reproduced, see Table 3. According to eqn. (26), this implies that the defect layers (characterized by A and $B(x_{nc})$) are indeed correctly defined by the relationship given in eqn. (20). The melting point of EMSCs is described exactly with the aid of eqn. (22), reproducing its dependence on the concentration in the melt, and also, of course, the systematic depression of the maximum melting temperatures for increasing x_{nc}. In the regime $y > y_{min} \approx 27$–30, the PE networks have in fact a random chain-length distribution. The mean thickness of the crystal core of EMSCs (y_{th}, Table 3) and its dependence on x_{nc} correlates with the mean thickness of the X-ray-coherent regions (y_{exp} Table 3). The small strain modulus is fairly

TABLE 3A

Basic parameters: radiation-crosslinked PE

$T_m = 415$ K; $\Delta h(T_m) = 4060$ J mol^{-1}; $\Delta c = 4.188$ J mol^{-1} K^{-1}; $2\sigma_e/\Delta(T) = 2.11$
$A = 0.15$; $B_1 = 0.9$; $B_2 = 50$
$\chi^m = 0$

TABLE 3B

Theoretical and experimental data of PE networks

Rad./MeG	x_{nc}/mol%	Δh_{exp}/J g^{-1}	Δh_{th}/J g^{-1}	L_{exp}/nm	L_{th}/nm	y_{exp}/nm	y_{th}/nm	E_{exp}/MPa	E_{th}/MPa	Q_{exp}	Q_{th}
500	0.125	25	28	–	–	–	–	22.6	19.1	1.38	1.4
400	0.100	35	31	6.5	16.5	0.9	1.15	20	17	1.5	1.5
300	0.075	40	33	–	–	–	–	14.3	14.3	1.62	1.6
200	0.050	58	53	10	9.3	2.5	2.6	–	–	–	–
150	0.038	85	75	–	–	–	–	9.45	9.4	1.83	1.9
110	0.028	73	80	11	9.0	4.8	4.4	9.1	7.7	2.1	2.1
75	0.020	96	96	13.5	11	–	–	6.1	6.1	2.21	2.4
55	0.010	113	114			5.1	6.3	–	–	–	–

Key: L, long periods deduced from SAXS; E, elastic modulus; Q, degree of swelling.

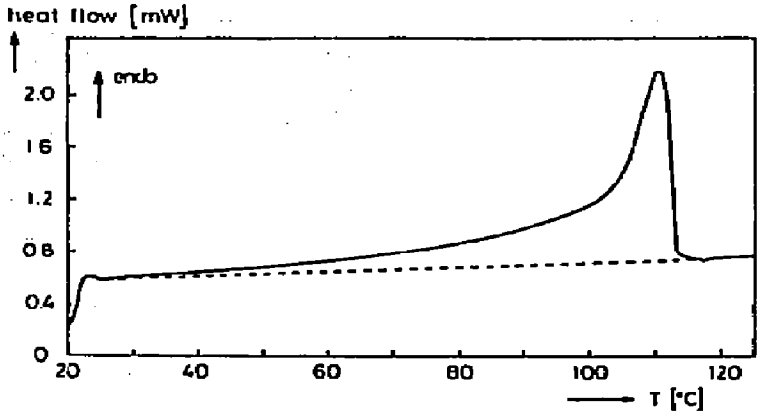

Fig. 16. A sketch of how the line should be constructed so as to separate the transition enthalpy from the total heat effect of a broadly melting copolymer [60, 61].

well computed (E_{th} and E_{exp}, Table 3). Hence, the effective number of tied molecules is correctly predicted, including its dependence on crystallinity.

The above results completely support the existence of equivalent sub-systems which are by definition self-similar [19, 59].

The C(y) distribution

We are faced with the problem that most copolymers do not show a random chain-length distribution. Therefore, it is extremely interesting that the $C(y)$ distribution can be deduced from an analysis of DSC melting curves.

First we have to separate the melting heats from the $c_p(T)$ curve (Fig. 16), see also ref. 60. The maximum degree of crystallinity is then given by

$$w_{cmax} \approx \frac{\Delta h_{exp}}{\Delta h_{max}} \tag{27}$$

The molar fraction of non-crystallizable units x_{nc} is assumed to be known from other methods.

The analysis is based on the phenomenon that EMSCs melt consecutively. Accordingly, a well defined fraction of EMSCs has to melt in each temperature interval ΔT [58, 61]. It is therefore appropriate to define a sufficiently large number of intervals ΔT. Thus, the calculation starts with a distribution $C_0(y)$ that is assumed to approximate as closely as possible the true c-sequence length distribution. This is not a necessary condition, but it helps to reduce the computer time. If the calculation differs from the experiment, the concentration of the c-sequences involved is modified accordingly. This adjustment is done in each temperature interval. After the first run, the mole fraction of nc-units is then no longer equal to x_{nc}. Renormalization is achieved by simply modifying the fractions in the

TABLE 4

Parameters of $-O(CH_3)-$ copolymers with $-O(CH_2)_n$ nc-units

$T_m = 456$ K; $\Delta h(T_m) = 9340$ J mol^{-1}; $\Delta c = 4$ J mol^{-1} K^{-1}; $2\sigma_e/\Delta h(T) = 1.88$; $\chi^m = -0.045$
$A = 0.15$; $B_1 = 0.9$; $B_2 = 22$

regime of shortest c-sequences that cannot crystallize ($y > y_{min}$). With the modified $C_1(y)$, the same program starts again. This is repeated until an optimum fit to the experiment is achieved.

Examples

Oxy-methylene copolymers comprising $-O(CH_4)_n-$ as nc-units ($n = 4, 6$) are interesting systems in which the co-units are "non-crystallizable" because they are not compatible with the $[-O(CH_2)-]_y$ lattice (Table 4); the x_{nc} value was known from the synthesis. Figure 17 shows the bimodal distribution, displaying a steep, relatively narrow peak in the range $y > y_{min}$. The distribution in the short-chain regime cannot be exactly determined.

This suggests that the bimodal distribution $C(y)$ results from the polymerization process. First, oligomers are built up and crystallize as soon as they are long enough. A rapid topochemical reaction is initiated on the lateral surfaces of these EMCs. By definition, the nc-monomers are not adsorbed here. Being squeezed out into the interlayers or into the melt, they become linked in chains there. Hence, very short c-sequences are formed in clusters and bound to longer sequences. The longer c-sequence length distribution should then reflect the thickness distribution of oligomer mixed EMCs nucleated at the beginning of the polymerization.

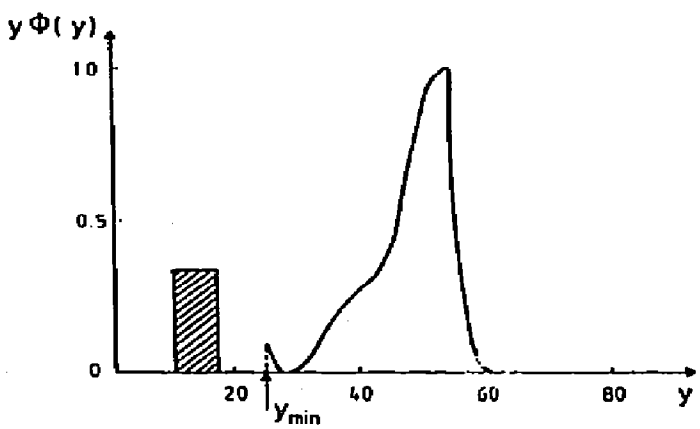

Fig. 17. Bimodal c-sequence length-distribution of $-O(CH_2)$-containing copolymers with $-O-(CH_2)_4$ nc-units ($x_{nc} = 0.031$). The hatched bar in the range $y < y_{min}$ represents the total mass fraction of non-crystallized c-sequences [58].

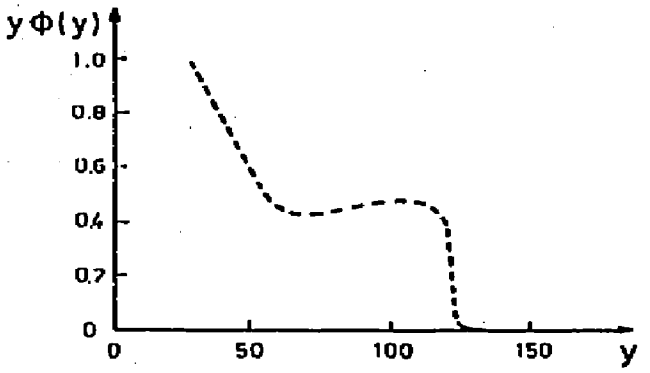

Fig. 18. The c-sequence mass distribution $y\phi(y)$ in low-density polyethylene [62].

According to such an analysis, low-density polyethylene should not show a random $-CH_2$ chain-length distribution (Fig. 18). In comparison with a random copolymer, there is a maximum in the regime of long c-sequences [58, 61]. This maximum seems not to be due to folded chain crystals.

In any case, the thermal analysis allows the c-sequence length distribution, even in networks, to be deduced from a DSC trace. Hence, an interesting analytical characterization of copolymers is possible which is difficult to assess otherwise.

However, even the longest c-sequences should not allow folded-chain crystallization. The utility of our method relies on the structure–chain-structure interrelationship

$$C(y) = C(y_{EMCS}) \qquad y \geq y_{min} \tag{28}$$

This relationship has been confirmed for branched polyethylene by investigating high-pressure crystallized samples [62]. Moreover, a line profile analysis of X-ray interferences performed using a known method [63, 64] has shown that the shape of the X-ray-coherent blocks is always nearly identical. The width and thickness of the X-ray-coherent cores and blocks of EMSC show about the same size distribution.

Clusters

Electron microscopy has shown (Fig. 19) that in random copolymers, lamellae-shaped EMSCs are arranged like particles in a dense gas. Strongly distorted clusters appear in which EMSCs of different thickness seem to be mixed at random [15, 58, 65, 66]. $C(y)$ is known from the thermal analysis. Non-crystallized layers are alternated with EMSCs. A Gaussian distribution should describe the thickness fluctuations of the non-crystallized layers. Accounting for the boundaries, a SAXS pattern can be computed by generating one-dimensional clusters comprised of a finite number of elements N (Fig. 20).

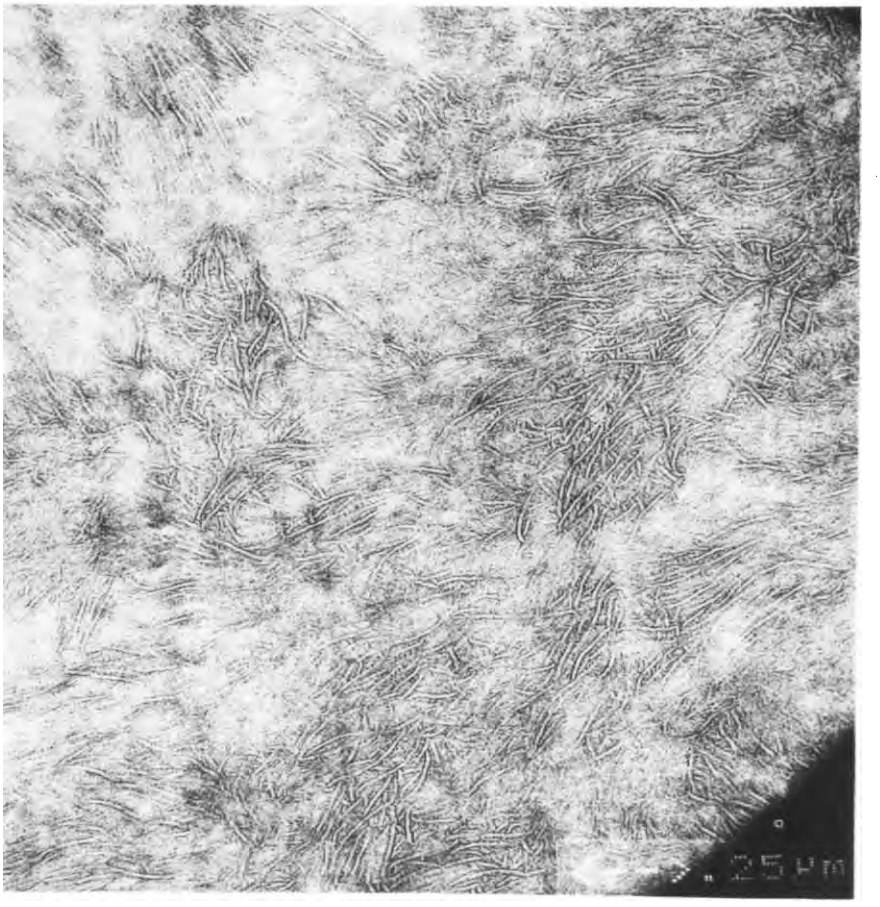

Fig. 19. Electron micrograph of a stained sample of a polyethylene network.

The quality of the fit to experiments on poly-oxy-methylene copolymers can be seen from the plot in Fig. 21. The finite number of EMSCs per cluster $N(T)$ determines the intrinsic constructive interference in the lamellae gas. It can be seen from Table 5 that the number N decreases with decreasing degree of crystallinity. At elevated temperatures, the width of the $C(y(T))$ distribution is diminished due to selective partial melting of the smallest EMSCs. The maximum in the SAXS pattern becomes pronounced until, at highest temperatures, one sees particle scattering of a diluted lamellae gas ($N \approx 1$) [67, 68]. One should comment on the fact that the theoretical SAXS curves at elevated temperatures are related to the room temperature pattern. They were calculated using the known set of thermodynamic parameters without any other adjustments. It must, of course, be known how the densities i the melt and in the crystals change with temperature. Two more examples of SAXS patterns, together with their theoretical representations, are depicted in Fig. 22.

The above description is based on the occurrence of selective and consecutive melting of EMSCs. Moreover, the whole configuration of

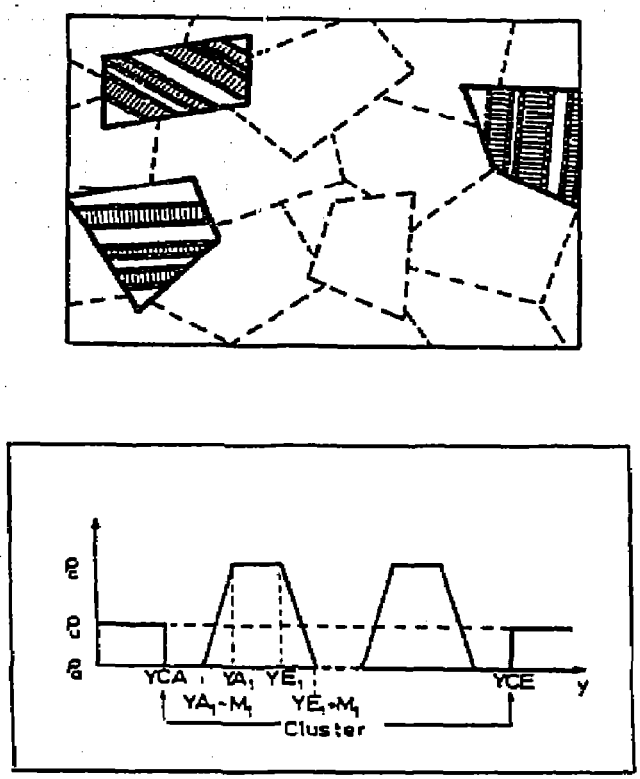

Fig. 20. Density projection onto the extremely flat Ewald-shell in the SAXS range of a cluster ensemble, yielding a very dilute cluster gas.

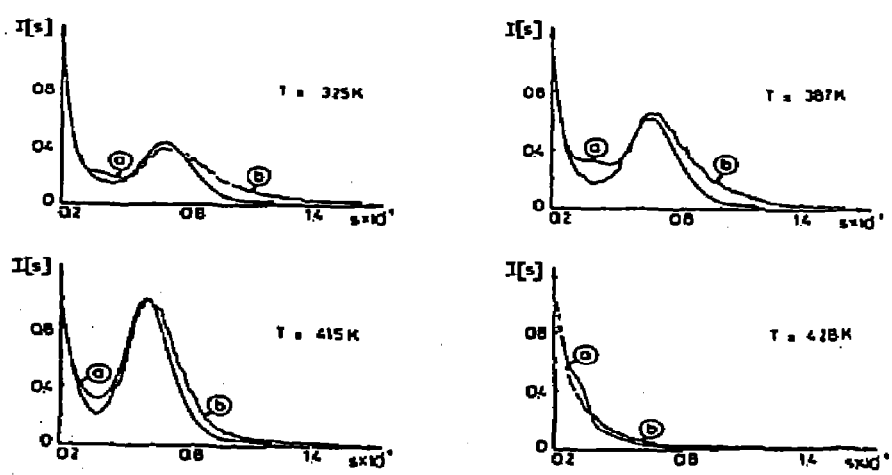

Fig. 21. Synchrotron SAXS pattern of $-(OCH_2)$-containing copolymers with $-O(CH_2)_4$ nc-units ($x_{nc} = 0.031$) at the temperatures indicated; curves a, theoretical patterns [58]; curves b, SAXS pattern obtained.

TABLE 5

Cluster-size parameter N for $-O(CH_2)$ copolymers with $-O(CH_2)_4$ nc-units: $x_{nc} = 0.031$, $w_{c,min} = 0.46$

T/K	325	387	415	428
$\langle N \rangle$	3.3	3.1	≈2	≈1.0

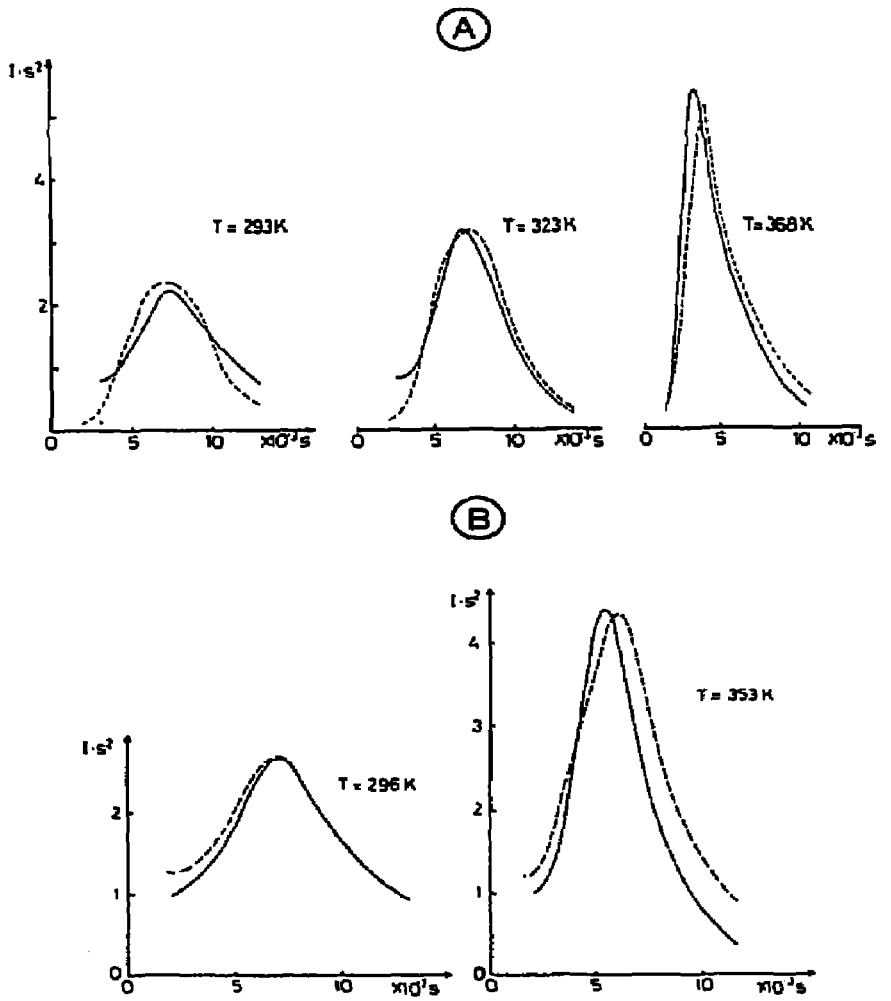

Fig. 22. Synchrotron SAXS data of (A) LDPE 1810 D and (B) vicinal chlorinated PE at the temperatures indicated (---); solid lines show computed data [58].

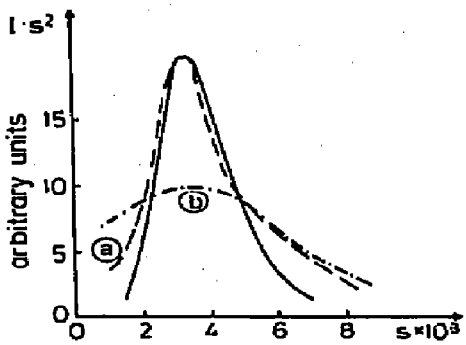

Fig. 23. SAXS pattern of LDPE (80 Mrad) at $T = 360$ K: —, experimental; – – – and ·–·–·–, theoretical. The gas model without memory effects fits the experiment (curve a). Curve b is the calculation with the "static cluster model" where EMSCs melt selectively without any rearrangement of the clusters.

EMSCs should be rearranged at each temperature. No memory effect seem to exist. The colloid structure in copolymers is continuously and reversibly modified with temperature. This is a necessary condition for the correct description of the temperature dependence of the SAXS pattern [69]. The intrinsic cluster-structure as well as the overall cluster configuration in copolymers with a broad ESMC distribution displays characteristics of a "dense gas" (Fig. 23) because of satisfying the maximum entropy principle.

The minimum size of the thermodynamically equivalent sub-systems should at least be larger than the mean cluster thickness which amounts to about 100 nm. But, this is only a rough estimate. It is more reasonable to postulate that each of the sub-systems should at least occupy a sufficiently large volume that $C(y)$ is fully represented. This condition cannot be fulfilled within a single cluster.

Crystallization kinetics

It is a well known feature that melting and crystallization deliver different DSC traces, see Fig. 25, below. Let us explain here an approach with which nucleation in eutectoid copolymers can be described in general [13, 18] using ideas from other publications [3, 70–79]. The crucial point is that both, temperature- and strain-induced crystallization, can consistently be explained.

In eutectoid copolymers with broad $C(y)$ values, it would seem that nucleation takes place without the appearance of crystal growth. In general, this should also be true in networks. To nucleate the mixed micro-phases, the mass balance between the coexisting phases can just be achieved locally within each of the equivalent sub-systems, without providing reliable opportunities for crystal growth.

We assume the nuclei with a thermodynamically determined thickness

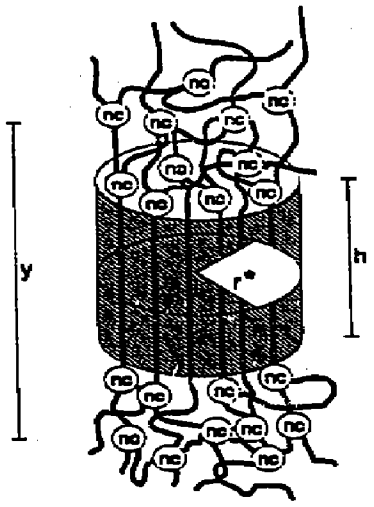

Fig. 24. Sketch of an EMSC nucleus. The thickness of the nucleus is thermodynamically determined. The defect boundaries are accounted for ($h = y - \Delta y/3$). The critical size is determined by the minimum radius r^*.

$y_u(T)$ must be formed. They represent themselves as inhomogeneous mixed micro-phases. The super-cooling is related to the melting temperature $T_{y_u(T)}$ at a given concentration in the metastable melt. The degree of supercooling must thus be related to the chemical potentials of these micro-phases. Simplifying the description, it is assumed that each nucleus has the same composition as the stable EMSC. A sketch of such a nucleus is depicted in Fig. 24.

It was shown elsewhere [18] that the nucleation rate in a eutectoid multi-component system is given by

$$I_{y_u(T)} = x^m_{y_u(T)}(t)\,\frac{RT}{\Delta h(T)}\{f_1 + [y_u(T)(x^m_{y0}(T) - x^m_{y(T)}(t))]^n f_2\}e^{-\Delta\mu^*_{ymu}/RT}e^{-\Delta G_n/R(T-T_0)}$$

$$\Delta\mu^*_{ymu} = \left(y_u(T) - \frac{\Delta y_v}{3}\right)^2 \frac{\sigma^2_M \pi}{\Delta\mu_{y(T)u}} \qquad (29)$$

$$x^m_{y0}(T) = \frac{x_y}{1 - e^{y_u(T)-1}}$$

$$r^* = \frac{y_v(T) - \Delta y_u/3}{\Delta\mu_{y(T)u}}$$

where f_1 and f_2 are phenomenological parameters where f_1 indicates homogeneous nucleation and f_2 accounts for secondary effects that depend on the fraction of nuclei that have been formed; n introduces a power law whereby this parameter must be adjusted; $x^m_{y0}(T)$ is the total mole fraction of c-sequences, while $x^m_{y_u(T)}(t)$ describes the momentary concentration of

c-sequences of length $y_u(T)$ in the multi-component melt; $\Delta\mu^*_{y_{nu}}$ gives the difference in the chemical potentials of c-sequences of length $y_u(T)$ in the nucleus and in the melt; σ_M is the lateral surface free enthalpy; $\mu_{y(T)nu}$ is the difference in the chemical potentials of the c-sequences in the metastable supercooled melt and in the equilibrium EMSC of thickness $y_u(T)$; $\mu_{y(T)nu}$ can be formulated analytically (see ref. 18), $T_{y_u(T)}$ is the melting temperature of EMSC nuclei of thickness $y_{nu}(T)$ in coexistence with the multi-component melt. Its momentary composition is continuously changed when nucleation proceeds, so that thermodynamic factors determine in a complex manner the nucleation rate of each nucleus of different thickness. ΔG_η related to the distance from the glass transition temperature T_{Gi}, describes in the traditional manner how the melt viscosity changes [3].

Thermally induced crystallization in PE networks

Here, we will discuss representative results. Figure 25 depicts the fit to DSC curves of polyethylene networks under a constant cooling and heating rate. Parameters are collected in Tables 3 and 6. The DSC traces are fairly well reproduced. Hence, it is in fact very likely that only nuclei are formed, with the same kinetic behaviour being shown for all EMSCs. The mass fraction of the coexisting micro-phases must always be correct within

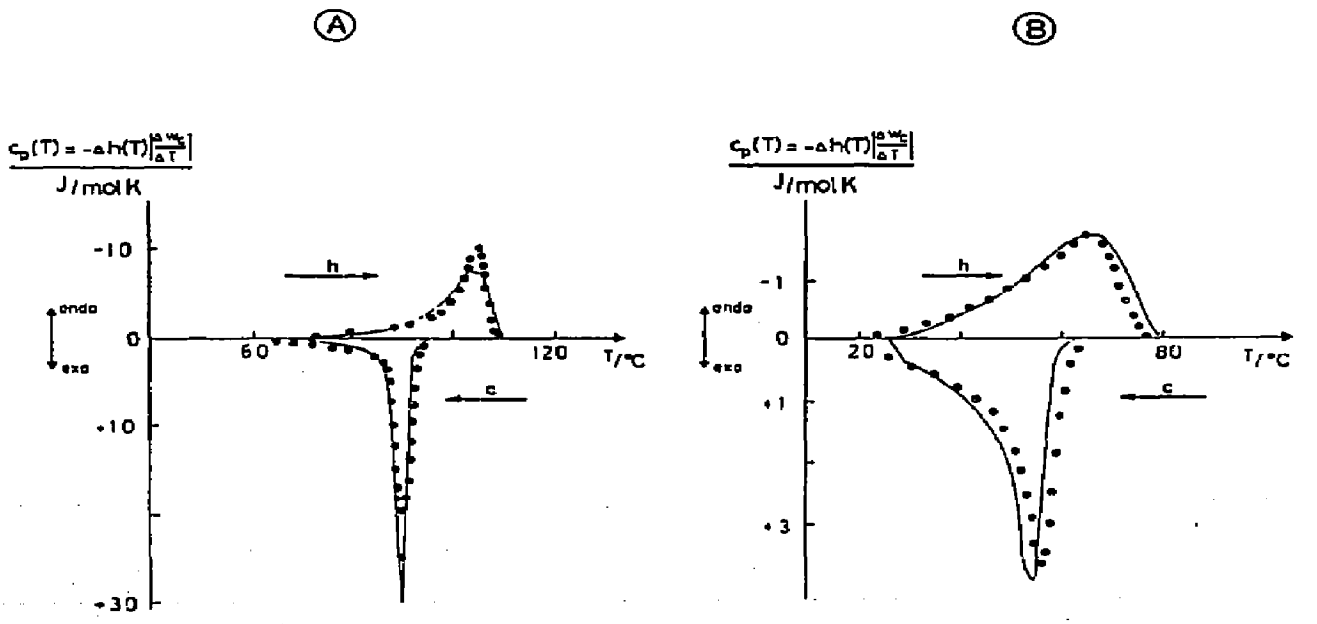

Fig. 25. DSC traces of radiation-crosslinked PE networks at a heating and cooling rate of 5 K min^{-1}: (A) 100 Mrad; (B) 400 Mrad. Solid lines are computed; parameters are given in Tables 3 and 6 [13, 18].

TABLE 6
Kinetic parameters of PE networks: $\sigma_M = \sigma_e/20$

dosis	x_{nc}	χ^m	f_1	f_2
100	0.0026	0.05	5×10^{-4}	1.5
400	0.067	0.2	1×10^{-4}	0.3

each of the sub-systems so as to fix uniquely in time the density of the EMSCs therein. However, the difference between the f_i values in both networks is not readily understood. The same is true for the interaction parameters χ^m. Despite these shortcomings, some general conclusions can be deduced.

(i) The networks crystallize like eutectoid copolymers; the junctions are nc-units.
(ii) Crystal growth does not seem to have a substantial role.
(iii) The nuclei should have about the same composition as the stable EMSCs.
(iv) The nuclei are inhomogeneous micro-phases in which influence of the defect boundaries on the thermodynamic factor increases with decreasing thickness $y(T)$.
(v) In the examples considered, heterogeneous nucleation should be dominant.
(vi) The nucleation rate depends on the momentary concentration in the melt which indicates the importance of relative concentration fluctuations which should not be substantially modified as crystallization proceeds.
(vii) During cooling with a constant rate, well-defined fractions of different EMSCs are nucleated almost simultaneously. Yet, the rate of crystallization decreases with decreasing thickness of the nuclei. Hence, a nucleation of c-sequences of different lengths runs selectively and consecutively on the time scale.

Crystallization kinetics in natural rubber networks

As another example, we present results obtained for natural rubber networks. The temperature dependence of thermally induced crystallization in the unstrained network is well understood (Fig. 26). The typical sigmoidal bending of the isothermal crystallization is correctly reproduced (Fig. 27), but this is not due to secondary crystallization effects [3]. The sigmoidal bending is the consequence of different nucleation rates for EMCs of different thickness. The smallest EMSC needs a very long time for complete crystallization.

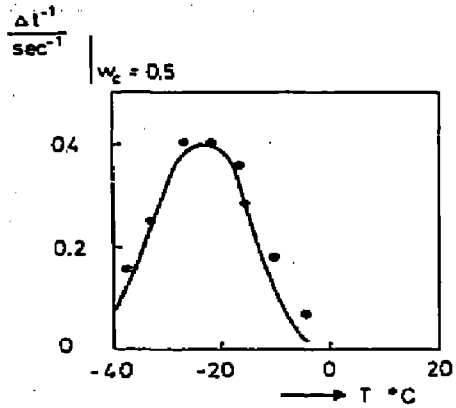

Fig. 26. Reciprocal time for reaching half the maximum crystallinity of a natural rubber network plotted against crystallization temperature, according to ref. 73. The solid line was computed [13, 18].

Strain-induced crystallization in natural rubber networks

It is in any case necessary to "overdraw" the network so as to enforce nucleation. We can describe the kinetic effects during strain-induced nucleation if the van der Waals network theory [17, 80, 81] is combined with the thermodynamics of eutectoid copolymers, Table 7.

Here, we confine ourselves to giving the stress–strain pattern and the heats exchanged during a stress–strain cycle (Figs. 28 and 29). The heats exchanged under quasi-isothermal conditions have been measured in a micro stretch-calorimeter [82–91]. According to the calculations, we understand fairly well the total energy balance that represents the exchange of work and heat during deformation. Even in a force field, c-sequence segregation in EMSCs with a thermodynamically defined thickness distribution takes place. The nucleation kinetics has features analogous to the

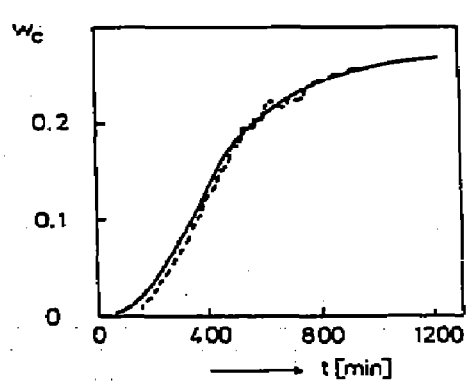

Fig. 27. The $w_c(t)$ of natural rubber ($x_{nc} = 0.02$) at $T = 248$ K. The solid line was computed [13, 18].

TABLE 7

Parameters for dicumyle-crosslinked natural rubber

$T_m = 298$ K; $\Delta h(T_m) = 4350$ J mol^{-1}; $2\sigma_e/\Delta h(T) = 2.06$; $\Delta c = 6$ J mol^{-1} K^{-1}
$A = 0.2$; $B_1 = 3.5$; $B_2 = 40$
$M_u = 36$ g mol^{-1}; $\lambda_{max} = 10.5$; $a = 0.287$
Kinetic parameters of NR networks
$\sigma_M = \sigma_e/20$; $\Delta G_u = 1550$ J mol^{-1}; $T_G = 209$ K; $n = 0.66$
$x_{nc} = 0.02$

Crystallization	f_1	f_2
Thermally induced	0.0115	11.5
Strain-induced	1.15	11.5

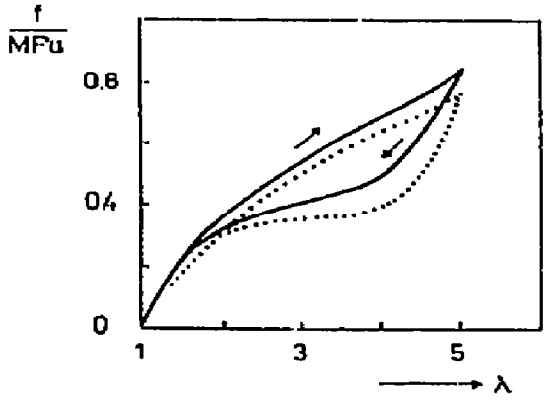

Fig. 28. The stress–strain cycle of natural rubber ($x_{nc} = 0.02$) at room temperature with the strain being increased stepwise, stopping in between for 20 min (this mode of deformation is optimal in the stretching microcalorimeter): · · ·, experimental; —, computed [13, 18].

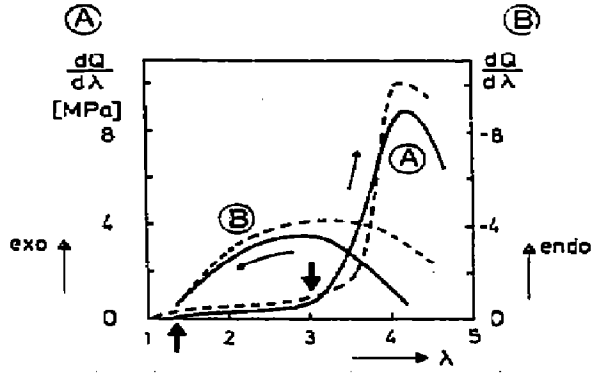

Fig. 29. Differential enthalpies $dQ/d\lambda$ ($x_{nc} = 0.02$) observed during the same cycle as shown in Fig. 28.

thermally induced nucleation only, in that nucleation runs within a relatively narrow $\Delta\lambda$ range.

It is not yet understood why strain-induced crystallization needs an f_1 parameter that is 100 times that for thermally induced nucleation in isotropic networks (Table 7). This effect might indicate that homogeneous nucleation of fully oriented crystals in oriented networks is greatly enhanced. Secondary nucleation, however, is not altered in either crystallization mode.

That networks must be overdrawn so as to enforce nucleation is clearly visualized from the asymmetry of the differential heats during a stress–strain cycle (Fig. 29). The broad melting process during unloading is a direct consequence of selective and consecutive melting of EMSCs that runs practically under equilibrium conditions. The same thickness distribution that occurs in the mode of thermally induced crystallization must exist. In the oriented equilibrium melt, EMSCs remain stable down to strains very much below those in which nucleation was enforced.

The size of sub-systems

From these results, it is clear that finite sized thermodynamically equivalent sub-systems should also exist in stretched networks. In oriented systems, these sub-systems must show on average the same composition as well as the same mean orientation of chain segments and EMSCs.

The size of the sub-systems can be estimated from the mean distance of the longest c-sequences ($x_c^{y_{max}-1}$). But we are interested in the relative distance D related to the dimensions of the mean end-to-end distance of a c-sequence of mean length in the copolymer, $(x_c/x_{nc})^{1/2}$.

$$D = \frac{\sqrt{x_c/x_{nc}}}{x_c^{y_{max}-1}} \qquad y_{max} \approx 6\frac{x_c}{x_{nc}} \tag{30}$$

It is reasonable to assume that the distance D is maximum at the critical mole fraction $x_{nc} \approx 0.015$–0.02, below which folded chain crystallization becomes more and more common. The data in Table 8 indicate that the maximum diameter of the sub-systems should range between 300 and 400 nm, which, for many reasons, appears to be a very reasonable order of magnitude.

TABLE 8

D dependent on x_{nc}

x_{nc}	0.10	0.075	0.05	0.025	0.02	0.015	0.01
y_{max}/nm	6.9	9.5	14.5	30.0	37.6	50.4	76.0
D/nm	100	130	179	284	325	385	482
						Chain folding	

Eutectic co-units

Let us once more discuss whether co-units behave like eutectic units. The possibility of smaller co-units being built into the crystal core of EMSCs has been discussed extensively in the literature [92–98]. The C=O unit is the only nc-unit that is built into the crystal lattice [99].

Fischer and coworkers have shown by SANS and SAXS measurements of chlorinated polyethylene that chlorines are included increasingly in the crystal core when the density of the chlorines increases (see also ref. 100). According to our model, chlorines should only be located in longitudinal surface layers. The density may here exceed that of the crystal core. The melting process of copolymers with vicinal chlorines is fairly well described, including their SAXS pattens, by assuming that these units cannot be built into the crystal core [69]. It might be expected that methyl branches, however, do not behave very differently because CH_3 units have about the same size as chlorines. This confirms that the depression of the maximum melting temperature cannot easily be used for identifying the role of nc-units. It can be seen from the plot in Fig. 30 that methyl or chlorine as short-chain branchings enforce a different melting point depression, despite having the same size. It has been suggested that this is due to the different excess properties in the melt [14].

It is important that we have derived a consistent description of the primary parameters of the colloid structure. These structure parameters are strictly determined by the $C(y)$ distribution. Their change with temperature is fairly well understood within the framework of the eutectoid copolymer model.

In the model of an inhomogeneous micro-phase, it is easy to squeeze all

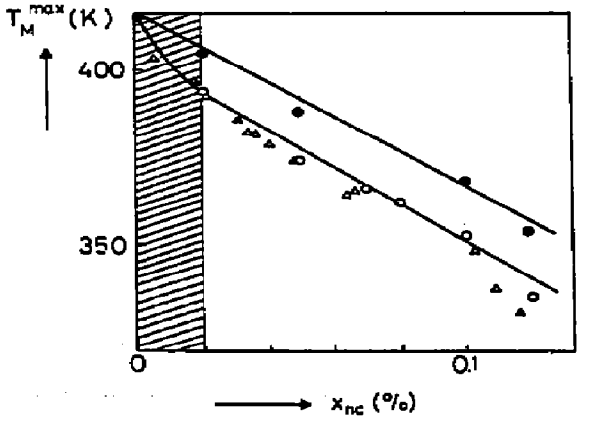

Fig. 30. Maximum melting temperatures of polymethylene copolymers as a function of composition and type of nc-units. The solid lines are computed (see refs. 14 and 94). ○, propyl; ●, methyl; and △, chlorine branchings.

the nc-units out of the core into the longitudinal defect layers. Even with the diffusion coefficient of a solid, these local arrangements are possible within a time interval of less than one second. Thus, it is unlikely that short-chain branchings can be restricted to the crystal core of EMSCs. This is supported by the observation that CH_3-branched *n*-alkanes cannot be built in EMCs of homologues.

Let us defend our interpretation by a simple, but instructive calculation. The defect layer of EMSCs includes nc-units. We have to translate this into the equivalent two-phase model. To this end, we first assume that the chlorines are homogeneously distributed across the non-crystallized regions (including the defect layers of the EMSCs). We may then define the partition coefficient of the chlorines, γ, by relating Δy to the mean thickness of the non-crystallized layers $\langle y^m \rangle$

$$\gamma = \alpha \frac{\Delta y}{\langle y^m \rangle} \qquad \langle y^m \rangle = \left(\frac{x_c}{x_{nc}} + y \right) \frac{(1 - w_p)}{w_p} \qquad w_p = x_c^{y-1}[(y-1)x_{nc} + x_c] \qquad (31)$$

The empirical parameter α must be adjusted. The data in Table 9 shows that our artificial two-phase representation does in fact lead to the observed result, i.e. the concentration of chlorines within equivalent crystals increases with increasing numbers of chlorines. Because EMSC are cooperative units, thermodynamics allow an equivalent two-phase description to be used. But, in this "mode of description", it must be postulated that an increasing fraction of nc-units is built into the equivalent crystals.

This interpretation opposes conclusions drawn by Eby, Flory and others [95, 96, 101–105]. It is significant that most of these authors used a two-phase model.

FINAL REMARKS

The power of a quantitative thermal analysis of melting and crystallization is most impressively demonstrated with the first full calculation of the heating and cooling DSC traces of networks. A solid understanding of the melting and crystallization kinetics is possible, even during stress–strain

TABLE 9

Distribution of comonomer units in chlorinated PE

x_{nc}	γ_{exp}	γ_{theo}	w_c
0.01	1	0.94	0.58
0.015	0.86	0.86	0.54
0.032	0.49	0.56	0.41

$A = 0.15$; $B_2 = 42$; $\alpha = 0.45$.

cycles. The exceptional method here is the stretch microcalorimetry which allows the whole energy balance during deformation to be measured.

It is shown that the chemical structure of copolymers containing nc-units has a unique influence on the colloid structure provided only extended chain or extended c-sequence crystals are formed. The crucial point is that it is essential to squeeze nc-units out of well-ordered lattices. Then, limited solubility in the solid extended chain or extended c-sequence mixed micro-phases of multi-component systems is the thermodynamic reason why the primary level of the colloid structure and the chain structure are strictly interrelated. Defining the model of inhomogeneous micro-phases, adequate thermodynamics can be developed. The thickness of the micro-phases is uniquely determined by the c-sequences built into them. Because c-sequences of different lengths are homologues, a systematic treatment of multi-component systems is possible, including excess properties in the solid solutions. Thus, we can predict isobaric state diagrams of eutectoid copolymers in a multi-dimensional hyper-space.

We have not discussed the very broad scale of different types of copolymers [94]. But as long as folded-chain crystallization does not occur, one should succeed in arriving at an analogous characterization, as shown in this paper.

Our results are significant in many respects.

(i) The thermodynamic equivalence of micro-phases is fully guaranteed.
(ii) Once finite size effects have been accounted for, the topology of the state diagrams (phase rule) can be determined, as in classical systems.
(iii) The size of the resultant equivalent sub-systems seems to be the result of "self-organization" of an "optimized colloid structure".

Copolymers approach equilibrium because of the existence of these equivalent sub-systems. Their size should be in the range of about 300–1000 nm. The colloid structure constituted by these sub-systems is typical for crystallized copolymers. Within each of the thermodynamically equivalent sub-systems, melting and crystallization are synchronized by thermodynamics. The same phenomena as in classical systems were observed macroscopically.

Finally, we ask what do we actually know about the colloid structure in eutectoid copolymers. In random copolymers the crystal thickness distribution can be deduced from an analysis of the melting. Because of having broad defect layers, interaction between neighbouring EMSCs should be identical, independent of their thickness. Each EMSC congfiuration is thus assumed to have the same energy. Features of the superstructure should therefore primarily be controlled by orientation correlations resulting from packing the EMSCs together. Clusters are developed. In the given circumstances, one observes a gas-like cluster structure so that SAXS patterns can be described by means of simplifying models. The mean size

of the X-ray-coherent clusters seems indeed to be determined by filling the space and maximizing the configurational entropy.

The question is how this could be achieved. It is clear from the thermodynamics of mixed micro-phases that c-sequences within EMSCs are always exchanged according to the dynamics in mixtures. Hence, rearrangements within the sub-systems of even complicated configurations should easily be possible. In eutectoid copolymers these processes are sufficient for maximizing the global entropy of the cluster assembly. This also seems to hold true in semi-crystalline oriented networks.

The interpretation of many experiments, particularly the calorimetric measurements, suggests the existence of thermodynamically equivalent sub-systems. Yet, at present we have no reliable method for identifying these sub-systems directly. Obtaining this knowledge is a key step in understanding the structural organization. In eutectoid copolymers, it is likely that the colloid structure is such that global extremum principles are fulfilled, approaching the entropy-maximum limit of a cluster gas structure. A description as to how superstructures are developed in semi-crystalline polymer systems under different boundary conditions has yet to be made. The present paper might suggest the first steps towards this description.

REFERENCES

1 B. Wunderlich, Macromolecular Physics, Vol. 3, Academic Press, New York, 1980.
2 M. Hoffmann, M.H. Krömer and R. Kuhn, Polymeranalytik I, Thieme, Stuttgart, 1977.
3 L. Mandelkern, Crystallization of Polymers, McGraw-Hill, New York, 1964.
4 L.J. Young, Copolymer Reactivity Ratios, in J. Brandrup and E.H. Immergut (Eds.), Polymer Handbook, 2nd edn., Wiley-Interscience, New York, 1975.
5 G.E. Ham, Copolymerization, Encyclopedia of Polymer Science and Technology, Wiley-Interscience, New York, 1966.
6 J. Bollinger, J. Macromol. Chem., C16 (1977) 23.
7 B. Wunderlich, Angew. Chem., 80 (1968) 1009.
8 G. Tosi, Adv. Polym. Sci., 5 (1968) 451.
9 H.J. Harwood, Angew. Chem., 74 (1965) 404.
10 H.J. Harwood, Angew. Chem., 77 (1965) 1124.
11 P.J. Flory, Trans. Faraday Soc., 51 (1955) 848.
12 J. Roe, K.J. Smith and W.R. Kregbaum, J. Chem. Phys., 35 (1961) 1306.
13 W.R. Kriegbaum, R.J. Roe and K.J. Smith, Polymer, 5 (1964) 533.
14 W. Glenz, H.G. Kilian, D. Klattenhoff and F. Stracke, Polymer, 18 (1974) 865.
15 H.G. Kilian, Prog. Colloid Polym. Sci., 72 (1986) 60.
16 H.G. Kilian, K. Unseld, E. Jaeger, J. Müller and B. Jungnickel, Colloid Polym. Sci., 263 (1985) 607.
17 B. Holl, H.G. Kilian and H. Schenk, Colloid Polym. Sci., 268 (1990) 205.
18 R.N.J. Conradt, B. Heise and H.G. Kilian, Progr. Colloid Polym. Sci., 87 (1992) 1.
19 J. Mayer, W. Schrödi, B. Heise and H.G. Kilian, Acta Polymerica, 41 (1990) 363.
20 H.G. Kilian, Makromol. Chem., 116 (1968) 219.
21 G.I. Asbach, K.H. Drexhage, G. Heidemann, W. Glenz and H.G. Kilian, Makromol. Chem., 139 (1970) 115.
22 G.I. Asbach, H.G. Kilian and F. Stracke, Colloid Polym. Sci., 260 (1982) 151.

23 P.H. Geil, Polymer Single Crystals, Interscience Publ., Wiley, Sydney, 1963.
24 D.C. Bassett, Principles of Polymer Morphology, Cambridge University Press, Cambridge, 1981.
25 D.C. Bassett, Developments in Crystalline Polymers, Applied Sciences Publishers, London, 1982.
26 E.W. Fischer, Koll. Z. Z. Polym., 231 (1969) 458.
27 B. Wunderlich, Macromolecular Physics, Vol. 1, Academic Press, New York, 1973.
28 A. Keller, J. Polym. Sci., Part A, 2 (1955) 291, 351.
29 M.G. Broadhurst, J. Chem. Phys, 36 (1962) 2578.
30 P.J. Flory and A. Vrij, J. Am. Soc., 36 (1963) 3548.
31 V.B.F. Mathot, Polymer, 25 (1984) 579. Errata: Polymer, 27 (1986) 969.
32 V.B.F. Mathot, Thermal Characterization of States of Matter, in V.B.F. Mathot (Ed.), Calorimetry and Thermal Analysis of Polymers, Hanser Publishers, Munich, 1994.
33 H.B. Callen, Thermodynamics, Wiley, New York, Toppan Comp., Tokyo, 1960.
34 R. Haase, Thermodynamik der Mischphasen, Springer-Verlag, Berlin, 1956.
35 A.W. Porter, Proc. Roy. Soc. London, 80 (1907) 519; (1908) 457.
36 G.I. Asbach and H.G. Kilian, Polymer 32 (1991) 3006.
37 J.I. Lauritzen and J.D. Hoffmann, J. Res. Natl. Bur. Stand. Sect. A, 64(1) (1960) 73.
38 H.G. Zachmann, Koll. Z. Z. Polym., 231 (1969) 504.
39 B. Wunderlich, Thermal Analysis, Academic Press, San Diego, 1990.
40 M. Sawodny, G.I. Asbach and H.G. Kilian, Polymer, 31 (1990) 1859.
41 B. Holl, B. Heise and H.G. Kilian, Colloid Polym. Sci., 261 (1983) 978.
42 J. Maxfield and L. Mandelkern, Macromolecules, 10 (1977) 1141.
43 J.H. Magill in J. Brandrup and E.H. Immergut (Eds.) Polymer Handbook, 3rd edn., Wiley, New York, 1989.
44 I.G. Voigt-Martin, Adv. Polym. Sci., 67 (1985) 194.
45 V.B.F. Mathot and M.F.J. Pijpers, Polym. Bull., 11 (1984) 297.
46 M. Sawodny, G.I. Asbach and H.G. Kilian, Macromol. Chem. Macromol. Symp., 39 (1990) 229.
47 M.P.J. Richardson, P.J. Flory and J.B. Jackson, Polymer, 4 (1963) 221.
48 R.B. Richards, J. Appl. Polym., 1 (1950) 370.
49 R. Alamo, R. Domszy and R. Mandelkern, J. Phys. Chem., 88 (1984) 6587.
50 C.G. Vonk, in Proceeding Golden Jubilee Conference Polyethylenes, Polymer Sci. Library, The Plastics and Rubber Institute, Chameleon Press, London, 1983, D2.1.
51 F.J. Baltá Calleja and C.G. Vonk, X-ray Scattering of Synthetic Polymers, Polymer Sci. Library 8, Elsevier, Amsterdam, 1989.
52 J. Martinez-Salazar, M. Sanchez Cuestá and F.J. Baltá-Calleja, Colloid Polym. Sci., 265 (1987) 239.
53 J. Martinez-Salazar and F.J. Baltá-Calleja, J. Cryst. Growth, 48 (1979) 283.
54 C.G. Vonk, J. Polym. Sci. Part C, 38 (1972) 429.
55 I.G.Voigt-Martin, R. Alamo and L. Mandelkern, J. Polym. Sci. Polym. Phys., 24 (1986) 1283.
56 L. Michajlov, H.J. Cantow and P. Zugenmaier, Polymer, 12 (1971) 70.
57 V.B.F. Mathot, The Crystallization and Melting Region, in V.B.F. Mathot (Ed.), Calorimetry and Thermal Analysis of Polymers, Hanser Publishers, Munich, 1994.
58 H.G. Kilian, R. Rosenberger, G.I. Asbach, W. Wilke and M. Rodrigèz, Makromol. Chem., 189 (1988) 2627.
59 H.G. Kilian, Progr. Coll. Polym. Sci., in press.
60 V.B.F. Mathot and M.F.J. Pijpers, Thermochim. Acta, 151 (1989) 241.
61 R. Pollak, G.I. Asbach and H.G. Kilian, Colloid Polym. Sci., 269 (1991) 433.
62 G.I. Asbach, G. Bodor and H.G. Kilian, Colloid Polym. Sci., 267 (1989) 976.
63 A.R. Stokes, Proc. Philos. Soc. London A, 61 (1948) 382.
64 G. Bodor, Adv. Polym. Sci., 67 (1985) 166.

65 H.G. Kilian, Macromol. Chem. Macromol. Symp., 26 (1989) 393.
66 B. Holl, B. Heise and H.G. Kilian, Colloid Polym. Sci., 261 (1983) 199.
67 A. Guinier, X-Ray Diffraction in Crystals, Imperfect Crystals and Amorphous Bodies, W.H. Freeman, San Francisco, 1963.
68 R. Hosemann and S.N. Bagchi, Direct Analysis of Diffraction of Matter, North-Holland, Amsterdam, 1962.
69 B. Heise, H.G. Kilian and H. Schmidt, Coll. Polym. Sci., 259 (1981) 611.
70 P.J. Flory, J. Chem. Phys., 15 (1947) 397.
71 P.J. Flory, Science, 124 (1956) 53.
72 J.F.M. Oth and P.J. Flory, J. Am. Chem. Soc., 80 (1958) 1297.
73 L.R.G. Treloar, The Physics of Rubber Elasticity, Oxford University Press, London, 1949.
74 P.J. Flory, Principles of Polymer Chemistry, Cornell University Press, Ithaca, New York, 1953.
75 R.H. Doremus, B.W. Roberts and D. Turnbull (Eds.), Growth and Perfection of Crystals, Wiley, New York, 1958.
76 L. Mandelkern, J. Appl. Phys., 26 (1955) 443.
77 R.S. Bradley, Quart. Rev. (London), 5 (1951) 315.
78 J.D. Hoffmann, J.J. Weeks and W.M. Murphey, J. Res. Natl. Bur. Stand. Sect. A, 63 (1959) 67.
79 L. Mandelkern and F.A. Quinn, Jr., Abstracts, 234th Meeting of the Am. Chem. Soc., Chicago 1958.
80 H.G. Kilian, Polymer, 22 (1981) 209.
81 B. Holl, H.G. Kilian and G. Yeh, Colloid Polym. Sci., 263 (1985) 313.
82 F.H. Müller, and A. Engelter, Koll. Z. Z. Polym., 152 (1957) 15.
83 A. Engelter and F.H. Müller, Koll. Z. Z. Polym. 157 (1958) 89.
84 D. Göritz and F.H. Müller, Koll. Z. Z. Polym., 251 (1973) 251.
85 H.G. Kilian, G. Höhne, P. Trögele and H. Ambacher, J. Polym. Sci. Symp., 77 (1984) 221.
86 D. Göritz, J. Polym. Sci., Part B, Polym. Phys., 24 (1986) 1839.
87 D. Göritz and F.H. Müller, Koll. Z. Z. Polym., 241 (1970) 1075.
88 Yu. K. Godovsky, Polymer, 22 (1981) 75.
89 Yu. K. Godovsky and N.P. Bessonova, J. Therm. Anal., 38 (1992) 1233.
90 Yu. K. Godovsky, N.P. Bessonova and N.N. Mironova, Coll. Polym. Sci., 267 (1989) 414.
91 Yu. K. Godovvsky, Adv. Polym. Sci., 259 (1986) 75.
92 C.A.F. Tuijman, Polymer, 4 (1963) 259.
93 C.A.F. Tuijman, Polymer, 4 (1963) 315.
94 B. Wunderlich, Macromolecular Physics, Vol. 3, Academic Press, New York, 1980.
95 D. Bodily and B. Wunderlich, J. Polym. Sci., Phys. Ed., 4 (1966) 25.
96 L. Mandelkern, Polymer, 7 (1966) 7.
97 U. Kalepky, E.W. Fischer and P. Herchenröder, J. Polym. Sci. Polym. Phys. Ed., 17 (1979) 2117.
98 R.J. Roe and C. Gieniewski, Macromolecules, 6 (1973) 212.
99 G.C. Alfonso, L. Fiorina, E. Martecelli, E. Pedemonte and S. Russo, Polymer, 14 (1973) 373.
100 H.G. Kilian, H.Linz, F.H. Müller, H. Ringsdorff, Koll. Z. Z. Polym., 202 (1965) 108.
101 R.K. Eby, J. Appl. Phys., 34 (1963) 2442.
102 J.P. Colson and R.K. Eby, J. Appl. Phys., 37 (1966) 3511.
103 I.C. Sanchez and R.K. Eby, J. Natl. Bur. Stand. Sect A, 77 (1973) 353.
104 I.C. Sanchez and R.K. Eby, Macromolecules, 8 (1975) 638.
105 E. Helfand and J.I. Lauritzen, Macromolecules, 6 (1973) 631.